

NACA RM L52K04



RESEARCH MEMORANDUM

MAR 5 1953

TRANSONIC CHARACTERISTICS OF A 45° SWEEPBACK
WING-FUSELAGE COMBINATION

EFFECT OF LONGITUDINAL WING POSITION AND DIVISION OF
WING AND FUSELAGE FORCES AND MOMENTS

By Joseph M. Hallissy and Donald R. Bowman

Langley Aeronautical Laboratory
Langley Field, Va

CLASSIFICATION CANCELLED

FOR REFERENCE

Authority *Naca Res. Abs.* Date *11-14-56*

ARN-109

By *NB 11-30-56* See

NOT TO BE TAKEN FROM THIS ROOM

CLASSIFIED DOCUMENT

This material contains information affecting the National Defense of the United States within the meaning of the espionage laws, Title 18, U.S.C., Secs. 793 and 794, the transmission or revelation of which in any manner to an unauthorized person is prohibited by law.

NATIONAL ADVISORY COMMITTEE FOR AERONAUTICS

WASHINGTON
February 27, 1953

NACA LIBRARY
LANGLEY AERONAUTICAL LABORATORY
Langley Field



NATIONAL ADVISORY COMMITTEE FOR AERONAUTICS

RESEARCH MEMORANDUM

TRANSONIC CHARACTERISTICS OF A 45° SWEEPBACK
WING-FUSELAGE COMBINATIONEFFECT OF LONGITUDINAL WING POSITION AND DIVISION OF
WING AND FUSELAGE FORCES AND MOMENTS

By Joseph M. Hallissy and Donald R. Bowman

SUMMARY

An investigation has been conducted in the Langley 16-foot transonic tunnel on a body of revolution with a sweptback wing having its 0.25-mean-aerodynamic-chord point located at the maximum body diameter and also at 1.2 mean aerodynamic chords behind the maximum diameter. The fuselage had a fineness ratio of 10, while the 45° swept wing had an aspect ratio of 4.0, a taper ratio of 0.6, and utilized NACA 65A006 airfoil sections parallel to the plane of symmetry. Lift, drag, and pitching moments were measured at Mach numbers from 0.6 to 1.03 and at angles of attack to 26° at the lowest speeds and to 8° at the highest speeds. For the wing in the forward position, the forces and moments were measured, on the wing in the presence of the fuselage as well as on the complete configuration.

Results of the tests indicate that, below 8° angle of attack, moving the wing to the aft position did not affect the lift or drag of the wing-fuselage combination. At higher angles of attack the lift and drag were both reduced in the wing-aft configuration. The variations of pitching moment about the 0.25-mean-aerodynamic-chord point with lift were similar for the two configurations but had a more positive slope for the wing-aft model; about half of this change being due to the contribution of the fuselage alone relative to the pitch axis.

INTRODUCTION

There have been several indications (see, for example, refs. 1 and 2) that an improvement in the performance of configurations intended for operation at transonic speeds might be effected by a longitudinal change



of position of a sweptback wing relative to the fuselage. It was reasoned that the improvement would result from a reduction in unfavorable wing-fuselage interference, or perhaps from the attainment of favorable interference.

This paper presents the results of force measurements made on a wing-fuselage configuration with the 45° -sweptback wing mounted at two longitudinal locations on the fuselage. For the configuration with the wing in the normal or forward location force measurements are presented for the wing in the presence of the body as well as for the complete configuration. The Langley 16-foot transonic tunnel was utilized in this investigation. The recent repowering of this tunnel has provided a facility in which tests can be conducted in the transonic speed range at reasonably high Reynolds numbers.

SYMBOLS

C_D	drag coefficient, D/qS
C_L	lift coefficient, L/qS
C_m	pitching-moment coefficient, $\frac{M_{c/4}}{q\bar{c}S}$
\bar{c}	wing mean aerodynamic chord
D	drag
L	lift
M	Mach number
$M_{c/4}$	pitching moment about $0.25\bar{c}$
P	pressure coefficient, $\frac{P - P_0}{q}$
P_0	free-stream static pressure
p	local static pressure
q	free-stream dynamic pressure, $\rho V^2/2$

S	wing area
V	free-stream velocity
x	chordwise distance from leading edge of mean aerodynamic chord
α	angle of attack relative to test-section center line
ρ	free-stream density

APPARATUS AND METHODS

Tunnel.- These tests were conducted in the Langley 16-foot transonic tunnel, a full description of which is given in reference 3. The test section is the slotted transonic type and is octagonal in shape. The tunnel speed is continuously variable throughout the Mach number range.

Model.- The wing-fuselage model used is geometrically similar to that used in a number of investigations carried out in other facilities. (See refs. 4, 5, and 6 for examples of these investigations.) The wing has NACA 65A006 airfoil sections parallel to the air stream, 45° sweep of the quarter-chord line, a taper ratio of 0.6, and an aspect ratio of 4.0. Ordinates for the NACA 6A-series airfoil sections may be found in reference 7. The wing was designed to have no twist or incidence relative to the fuselage, and checks of the completed model indicated that these objectives were achieved to within $\pm 0.1^\circ$.

The transonic body of revolution was constructed of magnesium and has a basic fineness ratio of 12, but is cut off at five-sixths of the length in order to attach the model support sting, thus giving a fineness ratio of 10. Fuselage ordinates are given in figure 1.

The model was tested with the wings mounted in two positions. In the first configuration, hereinafter called the wing-normal configuration, the quarter chord of the mean aerodynamic chord was located at the maximum body diameter. In the second configuration, hereinafter referred to as the wing-aft configuration, the quarter chord of the mean aerodynamic chord was located 22 inches or 1.197c to the rear of the maximum body diameter. The actual change of position was accomplished by shifting the body forward while the wing and balance for obtaining forces and moments remained in the same relative position in the tunnel. The terms wing-normal and wing-aft configuration always refer to the complete wing-fuselage configuration in this paper.

Dimensional details of the model and a sketch showing the wing in both positions are shown in figure 1. Figure 2 is a photograph of the model installed in the test section.

For that part of the tests in which forces on the wings outside the fuselage were measured, the wing was attached to the balance and the fuselage was supported by the sting independent of the balance. In order that there should be no physical interference, a gap was maintained around the wing-fuselage juncture. This gap was not at the wing surfaces, but was some distance above and below the surfaces as sketched in figure 3. Tests of the wings outside the fuselage were conducted with the wings mounted in the normal position only.

Model support system.- The main model support is a single swept cantilever strut, details of which are given in figure 4. The model sting attached to the strut, diverged uniformly from the fuselage base rearward for 36 inches. When the fuselage was mounted in the forward position (wing-aft configuration) a 22-inch cylindrical section of sting was exposed. In order to make the sting shape the same in the vicinity of the fuselage base for both configurations, this cylindrical section was covered by a fairing 24.75 inches long with the same uniform divergence as the sting.

The angle of attack can be varied from -5° to 15° using a straight sting coupling. Added angle-of-attack range is obtained by using a 10° coupling in the sting as shown in figure 4. The sting support-strut is mounted on a circular-arc track, the geometric center of which is in the center of the air stream near the model. Thus, the model was near the center of the tunnel at all angles of attack.

Instrumentation.- An internal strain-gage balance was used to measure the forces and moments on the model. The estimated accuracy of the coefficient of lift is ± 0.01 and of pitching moment is ± 0.005 . Estimated drag-coefficient accuracy is ± 0.001 at low angles of attack, increasing to ± 0.005 at the highest angles of attack.

Throughout the tests an attempt was made to set the model at the exact angle of attack desired at each test point. To the indicated angle of attack was added a predetermined incremental angle due to load on the model support strut, sting, and balance. This incremental angle, which approached 2° under some conditions, was determined by a static calibration of model angular deflection as a function of pitching moment and normal-force loads, made with the model mounted in the tunnel. The estimated over-all accuracy in angle of attack was $\pm 0.1^{\circ}$. This estimate is based on the repeatability of deflection measurements made during the static calibrations of the model support.

The Mach number was determined on the basis of the calibration described in reference 3 which was made with the tunnel empty except for an axial static survey tube and the same supporting strut used in the present tests. Surveys of the Mach number along the test-section center

line in the vicinity of the model indicate variations not greater than ± 0.002 . Mach numbers in this report are given to the nearest 0.01.

The base pressure was measured by two tubes which terminated a few inches inside the base of the model and pressure was indicated on mercury manometer boards. The indicated pressure was photo-recorded. The estimated accuracy of measurement of base pressure coefficient is ± 0.005 .

Test conditions.- Data were obtained at thirteen Mach numbers from 0.60 to 1.03. Test points were taken at 2° increments from angles of attack of -2° to 26° at Mach number 0.6, and to 8° at Mach number 1.03. The allowable stress on the model support structure limited the angle-of-attack range at the higher Mach number.

Figure 5 shows the Reynolds number range for the test to be from 4.75×10^6 to 5.95×10^6 . These values are based on a mean-aerodynamic-chord length of 1.531 feet.

Although there is no control over the absolute moisture content of the air in an atmospheric wind tunnel such as the Langley 16-foot transonic tunnel, high stagnation temperatures may be used to offset the relatively wet air of the locality. Stagnation dew point was measured at all test points and this enabled a calculation of humidity conditions in the tunnel test section. It was determined that unsaturated free-stream conditions prevailed for almost every point during these tests. Because of the higher local velocities in the model flow field there are many instances of local supersaturation, but since it is indicated in reference 8 that considerable supercooling can occur for a short time without resulting in condensation shock, it is believed that the data are free from the effects of such phenomena.

Data reduction.- No wind-tunnel corrections were applied to the data. The slotted throat is designed with an open-wall to solid-wall area ratio in the test region such that, for all subsonic speeds, the wall interference should be zero. Presently available experimental evidence from the Langley 16-foot and 8-foot transonic tunnels and comparisons with interference-free sources of data indicate that this objective has been achieved for all subsonic Mach numbers up to and including a Mach number of 1.00 (refs. 9 and 10). At slightly higher speed, Mach number 1.02 or 1.03, some interference probably exists, as is indicated by these same references, but the amount and effect of this interference is believed to be very small.

The angle of attack used is that measured relative to the test-section center line. The lift curves pass so close to the origin that it is apparent that the average flow angularity experienced by the model was very small, and accordingly no correction has been made.

No tare determinations other than base pressure measurement were made in connection with these tests, and the basic drag data presented have not been modified by base pressure or other adjustments. This does not affect the validity of comparisons in this report, but care should be exercised if comparisons are made with other data. For certain of the analysis figures, however, the drag values have been adjusted as will be noted subsequently.

For certain of the figures the force data for the fuselage alone were subtracted from the wing-fuselage data in order to obtain data for the wing plus wing-fuselage interference. The fuselage-alone data needed for this process were obtained in separate tests, but are not reported in this paper as they are essentially the same as those reported in reference 5.

DISCUSSION

Comparison of Aerodynamic Characteristics of Wing-Normal and Wing-Aft Configurations

Lift.- Upon examining the basic lift data (fig. 6) it is immediately apparent that there are no important differences between lift curves for the two wing positions below the break in the curve at a lift coefficient of about 0.6; above the break the curves diverge somewhat. The wing-normal configuration shows the better characteristics, with the lift curve breaking less sharply, and, at some speeds, at a higher angle than the wing-aft lift curve. The differences at a given angle, however, are small. At the lowest Mach numbers tested, where it was possible to obtain data at the higher angles of attack, it can be seen that this gain of the wing-normal configuration disappears as the lift curve turns upward toward maximum lift. At an angle of attack of 26° at a Mach number of 0.60 the wing-aft lift coefficient is the higher. It is not possible to say whether this would also be true at higher Mach numbers.

Figure 7 shows lift-curve slopes obtained in these tests. The wing-normal and wing-aft lift curves being similar below 0.6 lift coefficient, an average lift-curve slope has been determined for the two configurations for the lift-coefficient range from 0 to 0.6.

Drag.- Figure 8 shows that with drag, as well as with lift, there are no significant differences between the two configurations for lift coefficients lower than 0.6. At higher lift coefficients, however, the drag at a given lift coefficient is less for the configuration with the wing in the normal location. This lower drag is most clearly shown in figure 9 where drag coefficient is plotted through the Mach number range

at constant values of lift coefficient. A study of individual test points, however, shows that, for a given combination of angle of attack and Mach number, the drag is less for the wing-aft configuration in about the same proportion as the normal force as indicated by the reduction in lift coefficient. Reference 11 indicates that this normal-force reduction occurs mainly on the outboard sections of the wing and is associated with a change in the position of the afterbody-shock location relative to the wing tip. Since for the wing-aft configuration the wing tips extend somewhat behind the model base in the longitudinal direction, it is possible that there is a sting interference effect on the outboard sections of the wing in this case which was not present for the wing-normal configuration. It is believed, however, that such an effect would be small and probably in the opposite direction to the observed differences.

The transonic-drag-rise increments were 0.011 at $C_L = 0$, 0.014 at $C_L = 0.2$, and about 0.019 at $C_L = 0.4$; these values apply for both configurations. The erratic behavior of the curves of drag coefficient at constant lift coefficient (fig. 9) for Mach numbers of about 0.85 to 0.90 is directly traceable to the characteristics of the lift curves. The minimum drag which occurs in the curves for $C_L = 0.4$ and $C_L = 0.6$ results from the increased lift-curve slope; whereas the maximum occurring for $C_L = 0.8$ appears because the lift curves break at lower lift values for these Mach numbers and thereby increase the angle of attack (and drag) required to obtain a given lift coefficient.

A comparison of maximum lift-drag ratios is made in figure 10. The maximums occur in the region of the lift-drag curves below 0.6 lift coefficient, so that the differences are almost insignificant. The data indicate a slightly higher $(L/D)_{max}$ in the Mach number range from 0.7 to 0.90 for the wing-normal configuration, and practically no difference at higher speeds. Drag data used in the preparation of this figure have been adjusted to the condition of free-stream pressure at the base.

Base pressure coefficient. - The variations of base pressure coefficient with Mach number, given in figure 11, were similar for all angles of attack up to about 12° . The base pressure coefficient for the body alone, wing-normal and wing-aft configurations generally increased with increased Mach number in each case, peaked near Mach number 1.0, and then dropped with further Mach number increase. The peak coefficient and the Mach number at which it occurred, however, depended on the configuration, both being highest for the body-alone configuration and lowest for the wing-aft configuration. It should be pointed out that these differences have a fairly small effect on the drag. A base-pressure-coefficient difference of 0.065, for example, corresponds to a drag-coefficient difference of 0.001. Most of the differences in base pressure coefficient between configurations are considerably less than this.

Pitching moment.- The pitching moments for the complete configurations, shown in figure 12, were measured about the quarter chord of the wing mean aerodynamic chord for both the wing-forward and wing-aft tests. Center-of-pressure locations measured from this moment axis are given in figure 13 as a function of Mach number. Three important results are indicated by these figures: First, the unstable break in pitching moment which is characteristic of the sweptback wing and which occurs at lift coefficients around 0.6 for this wing is little affected by the change in the longitudinal location of the wing. Second, the variation of the center-of-pressure location with Mach number is seen to be almost identical for the two configurations at a given angle of attack. Third, the pitching-moment curve for the wing-aft configuration has a less stable slope than the pitching-moment curve for the wing-forward configuration under nearly all conditions. This result was expected inasmuch as the contribution of the fuselage to the total moment is fairly large and the fuselage was moved forward with respect to the moment axis. The actual extent to which the center-of-pressure location was shifted forward by changing the wing to the aft position is seen in figure 13 to be about five percent of the mean aerodynamic chord for most conditions.

In order to determine whether this moment change is due merely to the increased positive moment contribution of the body alone as it is moved forward with respect to the moment axis (in the wing-aft configuration), the lift and moment for the wing plus wing-fuselage interference were determined. This information is presented in figure 14 and was obtained by subtracting the body-alone data from the combined wing-fuselage data. The resulting moment curves have a more negative slope than those for the complete configurations, particularly for the wing-aft model. The difference in slopes is thus reduced but not eliminated, indicating that only part of the difference in slope for the two complete configurations is due to an increase in the body-alone contribution. The latter observation is emphasized in figure 15, which shows the longitudinal center of pressure for the wing plus wing-fuselage interference. The forward shift of the center of pressure for the wing-aft model is from 1.5 to 5 percent of the mean aerodynamic chord, with most conditions indicating 2 to 3 percent shift. Thus, only about half of the difference in pitching-moment slope was due to the change in body-alone contribution caused by a shift in the body position with respect to the wing. The remainder represents a forward shift in loading on the wing itself or in the wing interference loading on the fuselage. This forward shift in wing loading is more clearly shown in data presented in reference 11.

At a Mach number of 0.6 where data could be obtained at high angles of attack, there appears to be a discrepancy in the shape similarities between the pitching-moment coefficients for the two complete configurations. The curve for the wing-normal model shows a sharp stable break at a lift coefficient of 0.89; whereas that for the wing-aft model continues

to rise to the highest lift coefficient obtained which was 1.01. However, when the body-alone data are subtracted from the combined data to give lift coefficient for the wing plus wing-body interference, this discrepancy no longer appears, and both configurations show the stable break at a lift coefficient of about 0.83 (fig. 14). This break is present for both configurations, but is masked in the combined pitching-moment curve for the wing-aft model by the large positive pitching-moment contribution of the body alone.

Aerodynamic Characteristics of the Wing Outside the Fuselage

Lift.- It is usually assumed that the percentage of the total lift contributed by the fuselage is roughly the same as the percentage of the wing area blanketed by the fuselage. If this rule of thumb is applied to the present case, the lift of the wing outside the fuselage shown in figure 16 could be expected to be about 83 percent of the total lift since in the present case the area covered by the fuselage is slightly less than 17 percent. As shown in figure 17, the relationship applies with a fair degree of accuracy over a wide range of conditions for the present configuration. Figure 17(a), which uses the lift-curve slope ratios as an indication of load distribution, is applicable for the linear portion of the lift curve and indicates that from 81 to 88 percent of the total load is carried by the wing. At 0.8 lift coefficient, as indicated by figure 17(b), the wing lift was 82 to 85 percent of the total lift. At higher angles of attack than about 16° , however, figure 16 shows that the wing lift drops somewhat, being 75 percent or less of the total at the highest angles of attack at Mach numbers 0.6 and 0.7. This is undoubtedly due to the fact that the outboard loading on wings of this type falls off or at least fails to increase further at these angles.

Drag.- Figure 18 shows the drag coefficient of the wing outside the fuselage as a function of total wing-fuselage lift coefficient at the several Mach numbers of the test. Since it is well known that the correction due to sting drag tare is an appreciable part of the total drag of a clean configuration at low-lift coefficient, and since the sting tares were not determined in the present case, it is not possible to obtain from these data a direct evaluation of the division of drag between the wing and fuselage. However, it is possible to evaluate this division of drag by making a comparison of the drag of the wing outside the fuselage with the drag of the complete configuration as determined by an interference-free technique. This evaluation has been made in figure 19 which shows the zero-lift drag coefficient of the wing outside the fuselage measured in the present tests compared with the total drag coefficient of a similar wing-fuselage configuration obtained by the rocket technique. The original rocket-test data, which were obtained from reference 6,

included the drag of two small stabilizing fins. For purposes of the present comparison an estimated fin drag coefficient of 0.001 has been subtracted out at subsonic speeds and 0.002 subtracted out at supersonic speeds. This comparison indicates that the zero-lift drag of the wing in the presence of the fuselage is about 40 to 50 percent of the total drag of the configuration at both subsonic and supersonic speeds.

No interference-free data are available for making similar comparisons at lift coefficient, but it is believed to be reasonable in the present case to make the assumption that the zero-lift sting drag tares are applicable throughout the angle-of-attack range. Figure 20 repeats the drag polars of figure 18 at five Mach numbers for the wing in the presence of the body and compares them with total wing-fuselage drag polar corrected for sting drag tares as indicated previously on the basis of the zero-lift rocket data. This comparison shows that the wing drag increases from 40 or 50 percent of the total at zero lift to 75 or 80 percent of the total at high lift coefficients. This increase in wing drag is not surprising since at high lift coefficients the induced drag constitutes most of the total drag, and the division of induced drag between wing and body would be similar to the division of lift.

Pitching moment. - The pitching-moment curves of figure 21 for the wing outside the fuselage are very similar in shape at all speeds to those for the complete configuration except for a considerably more negative slope. These similarities are to be expected since the non-linear characteristics of the moment curves for swept wings result from flow conditions on the outer parts of the wings. The center of pressure for the wing outside the fuselage, given in figure 22 for several angles of attack, indicates shifts of the center of pressure with Mach number for the wing outside the body which are nearly identical to those of the complete wing-fuselage configuration except for an over-all rearward displacement. The center of pressure for the wing outside the fuselage at 4° angle of attack, for example, shifts 15 percent from a low-speed location at $\frac{x}{c} = 0.38$ to a location at $\frac{x}{c} = 0.53$ at the highest Mach number obtained. Under the same conditions the center of pressure for the complete configuration shifts 15 percent from $\frac{x}{c} = 0.24$ to $\frac{x}{c} = 0.39$ (fig. 13).

CONCLUSIONS

An investigation of a 45° sweptback wing-fuselage configuration in the Langley 16-foot transonic tunnel indicates the following conclusions:

1. Effects of longitudinal position on the wing in two positions on the fuselage

(a) Below a lift coefficient of about 0.6 there were no appreciable differences in lift coefficient, but above this point the wing-aft results generally indicated somewhat lower lift-coefficient values at the same angle of attack.

(b) Drag coefficients obtained at lift coefficients below 0.6 were also negligibly affected by the change of longitudinal wing location, the variation of drag rise with Mach number being very nearly identical for the two wing positions. Drags at higher lift coefficients than 0.6 were adversely affected by moving the wing aft because of the reduced normal force which resulted in higher drags at the same lift coefficient for this configuration.

(c) Curves of pitching-moment plotted against lift for the two configurations were similar in shape but of different slope, the center of pressure being about 5 percent of the mean aerodynamic chord farther forward for the wing-aft configuration. About half of this difference, however, was due to the increased moment arm of the body-alone contribution which results when the wing position was changed.

2. Forces and moments on the wing in the presence of the fuselage

(a) The percent of the total wing-fuselage lift load carried by the wing outside the fuselage was about the same as the percent of total wing area which was outside the fuselage, which was 83 percent in this case.

(b) The percent of the total wing-fuselage drag which was measured on the wing outside the fuselage increases from 40 to 50 percent at zero lift to 75 or 80 percent at lift coefficients of 0.8 or higher.

(c) Rearward shifts in center-of-pressure location with increases in Mach number through the transonic-speed range for the wing outside the fuselage were nearly identical to those for the complete configuration.

Langley Aeronautical Laboratory,
National Advisory Committee for Aeronautics,
Langley Field, Va.

REFERENCES

1. Mathews, Charles W., and Thompson, Jim Rogers: Comparison of the Transonic Drag Characteristics of Two Wing-Body Combinations Differing Only in the Location of the 45° Sweptback Wing. NACA RM L7101, 1947.
2. Nelson, Robert L.: Large-Scale Flight Measurements of Zero-Lift Drag at Mach Numbers From 0.86 to 1.5 of a Wing-Body Combination Having a 60° Triangular Wing With NACA 65A003 Sections. NACA RM L50D26, 1950.
3. Ward, Vernon G., Whitcomb, Charles F., and Pearson, Merwin D.: Air-Flow and Power Characteristics of the Langley 16-Foot Transonic Tunnel With Slotted Test Section. NACA RM L52E01, 1952.
4. Cahill, Jones F., and Gottlieb, Stanley M.: Low-Speed Aerodynamic Characteristics of a Series of Swept Wings Having NACA 65A006 Airfoil Sections (Revised). NACA RM L50F16, 1950.
5. Osborne, Robert S., and Mugler, John P., Jr.: Aerodynamic Characteristics of a 45° Sweptback Wing-Fuselage Combination and the Fuselage Alone Obtained in the Langley 8-Foot Transonic Tunnel. NACA RM L52E14, 1952.
6. Katz, Ellis: Flight Investigation From High Subsonic to Supersonic Speeds To Determine the Zero-Lift Drag of a Transonic Research Vehicle Having Wings of 45° Sweepback, Aspect Ratio 4, Taper Ratio 0.6, and NACA 65A006 Airfoil Sections. NACA RM L9H30, 1949.
7. Loftin, Laurence K., Jr.: Theoretical and Experimental Data for a Number of NACA 6A-Series Airfoil Sections. NACA Rep. 903, 1948. (Supersedes NACA TN 1368.)
8. Oswatitsch, Kl.: Formation of Fog in Wind Tunnels and Its Influence on the Investigation of Models. Repts. and Translations No. 459, British M.A.P. Völkenrode, June 1946.
9. Hallissy, Joseph M., Jr.: Pressure Measurements on a Body of Revolution in the Langley 16-Foot Transonic Tunnel and a Comparison With Free-Fall Data. NACA RM L51L07a, 1952.
10. Ritchie, Virgil S., and Pearson, Albin O.: Calibration of the Slotted Test Section of the Langley 8-Foot Transonic Tunnel and Preliminary Experimental Investigation of Boundary-Reflected Disturbances. NACA RM L51K14, 1952.

11. Solomon, William, and Schmeer, James W.: Effect of Longitudinal Wing Position on the Pressure Characteristics at Transonic Speeds of a 45° Sweptback Wing-Fuselage Model. NACA RM L52K05a, 1953.

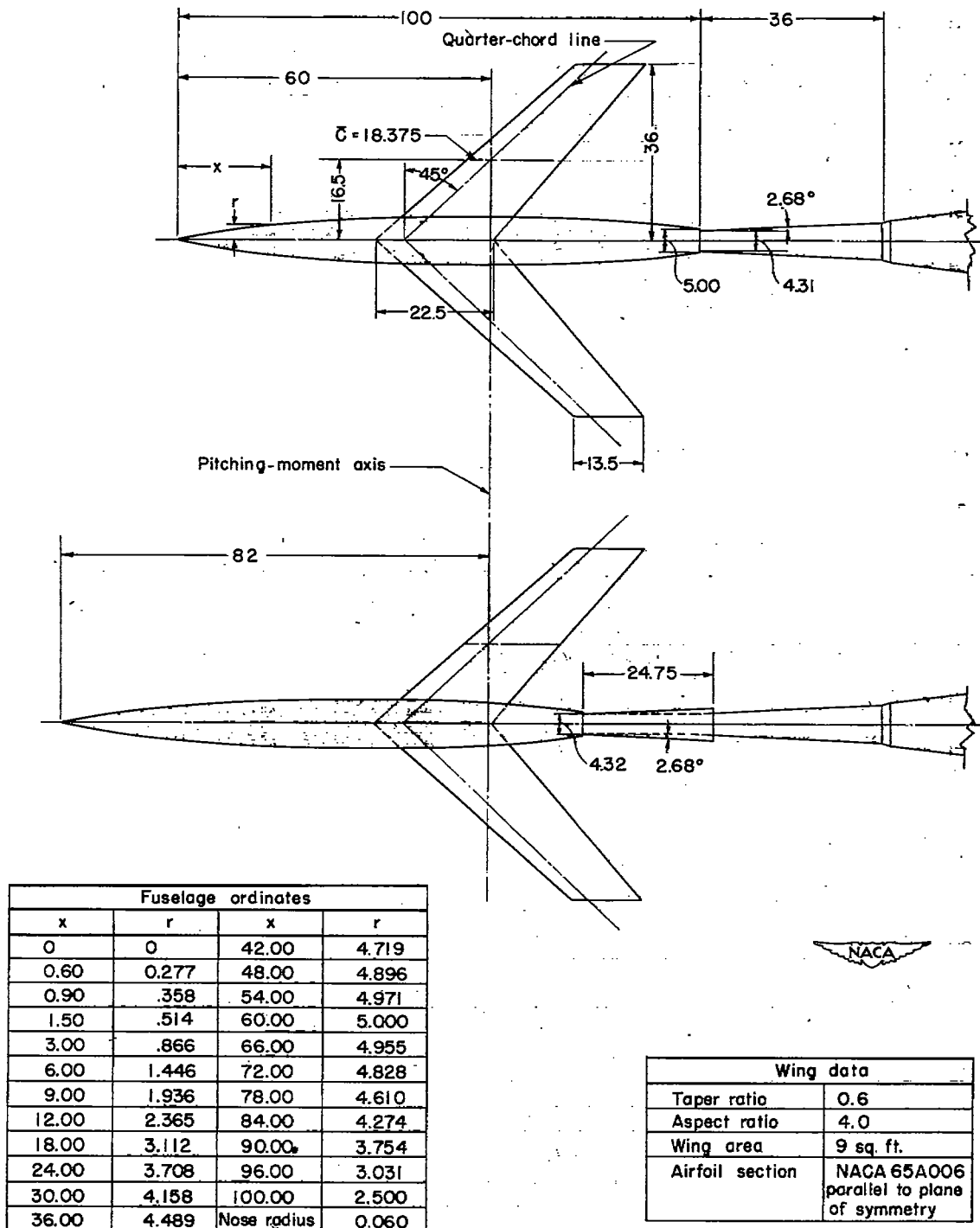


Figure 1.- Model dimensions and arrangement, wing-normal and wing-aft configurations. All dimensions are in inches.



Figure 2.- Wing-normal model installed in the Langley 16-foot transonic tunnel test section.

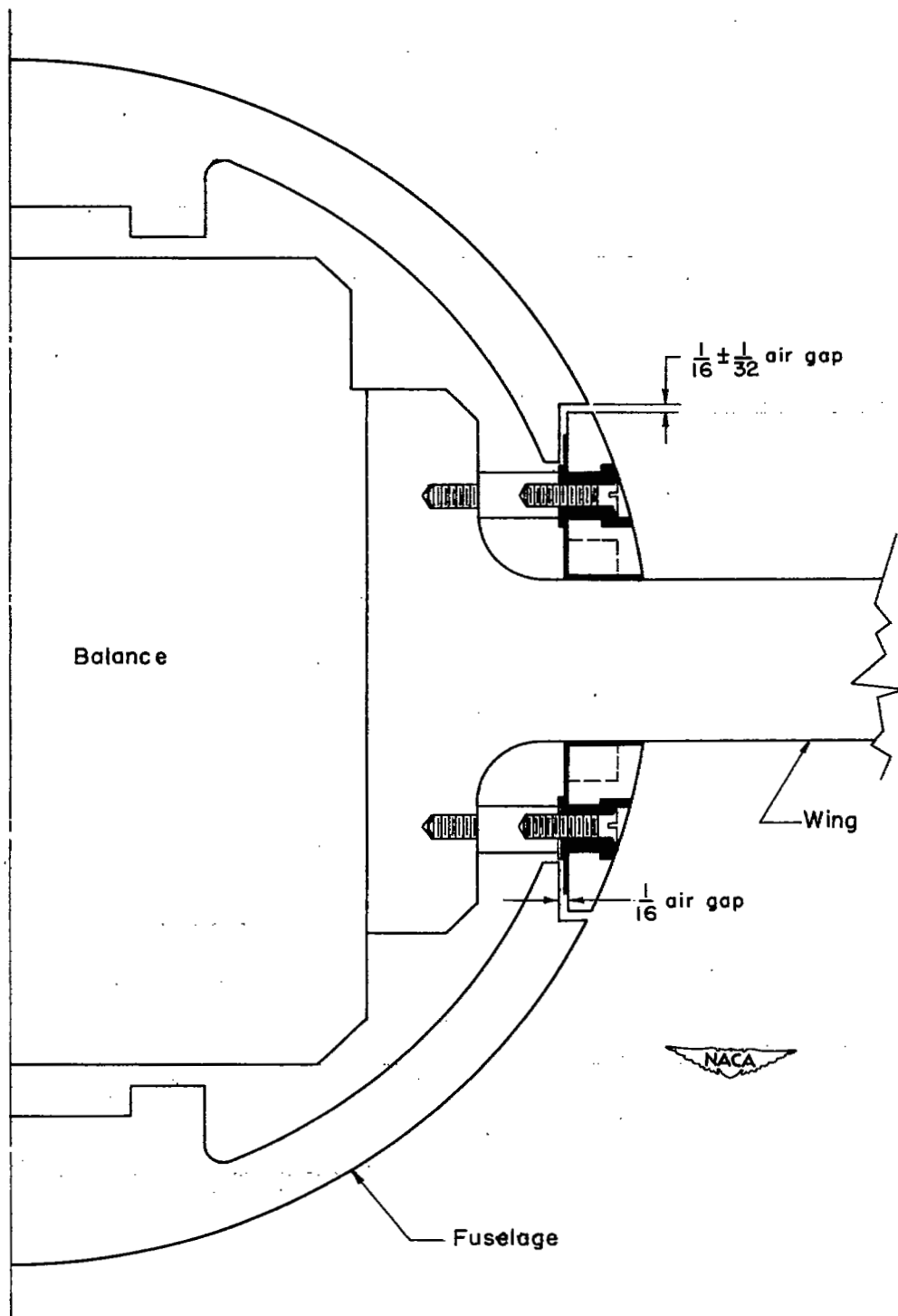


Figure 3.- Cross-section showing details of wing-fuselage juncture used when obtaining force data on the wing outside the fuselage.

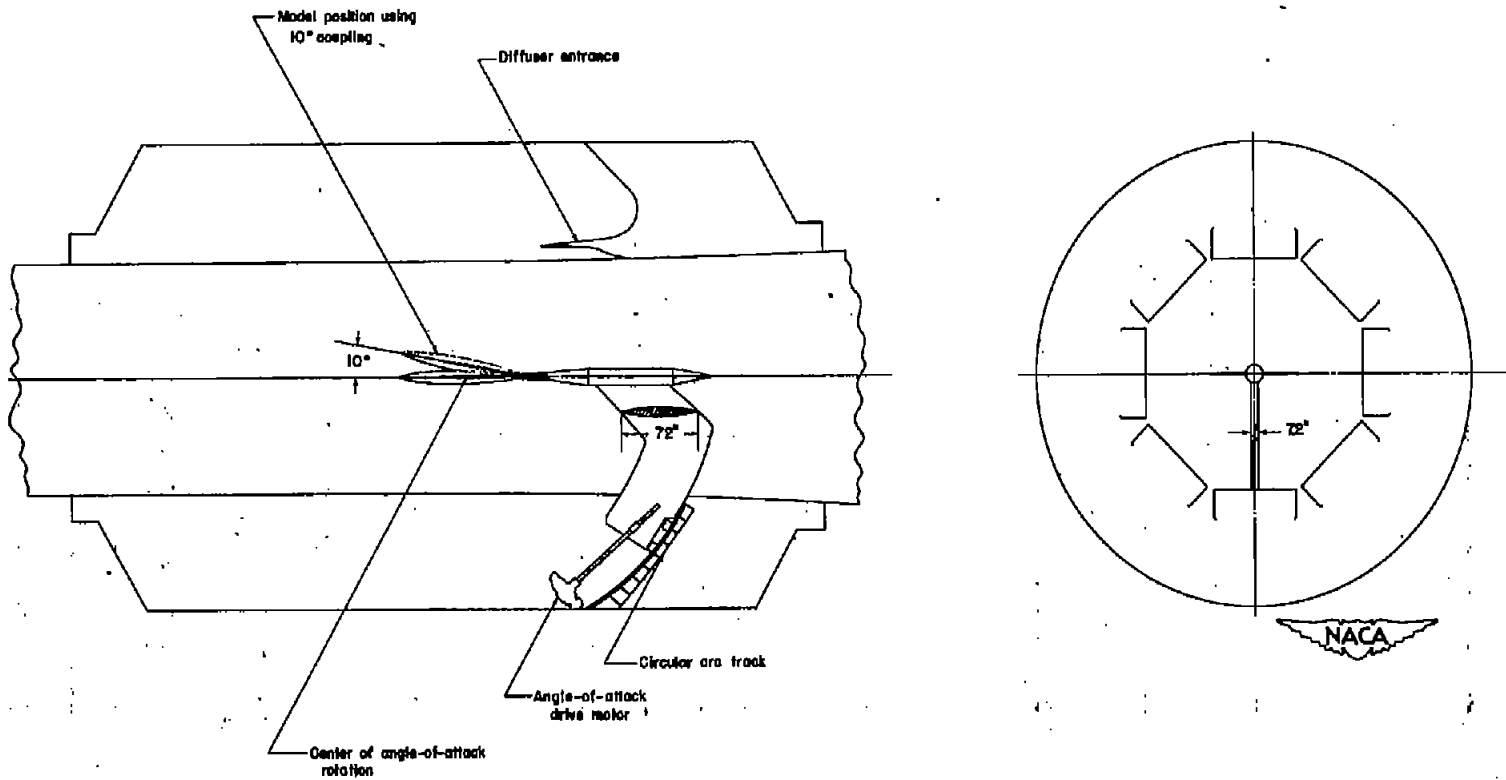


Figure 4.- Model support system in the Langley 16-foot transonic tunnel test section.

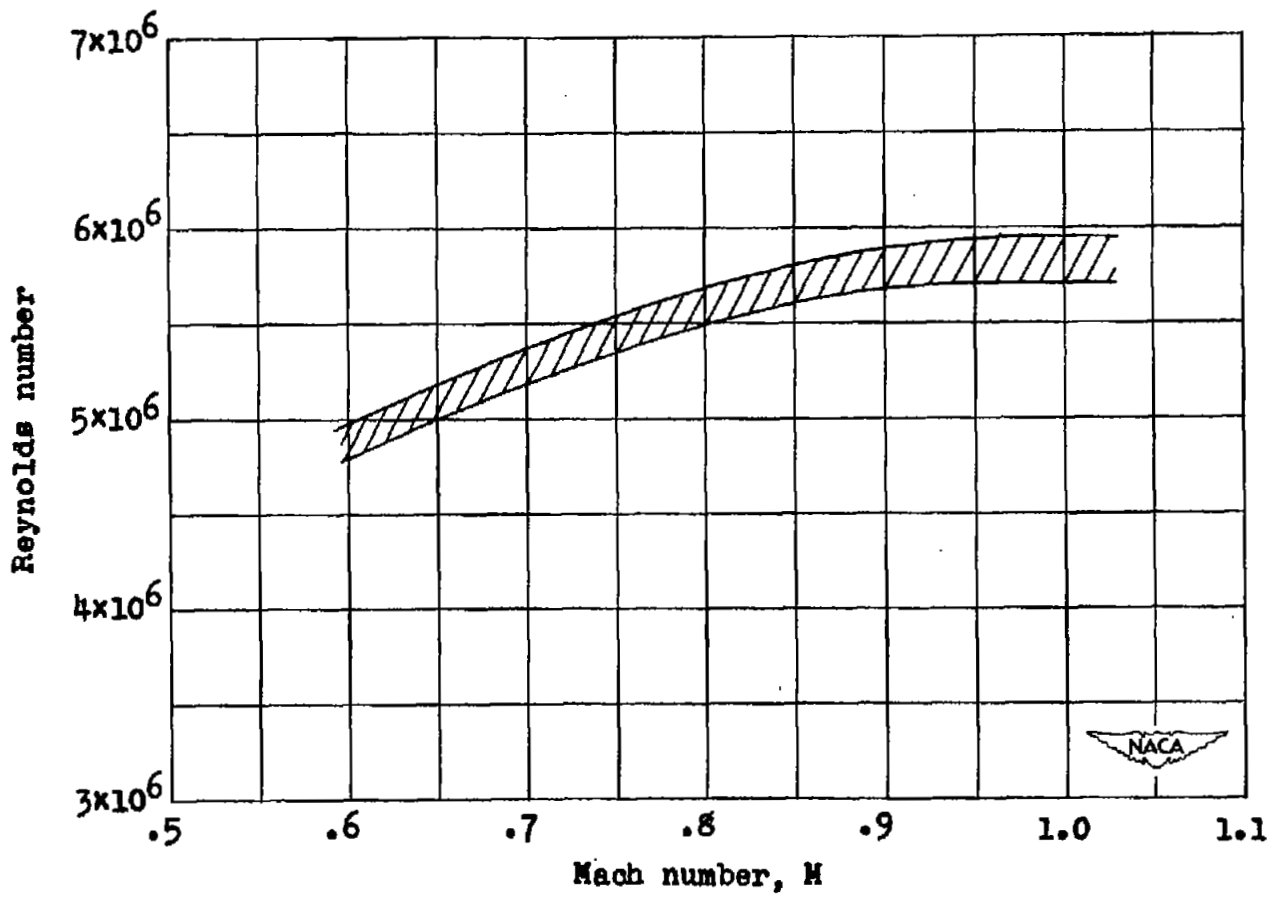


Figure 5.- Reynolds number range based on mean aerodynamic chord.

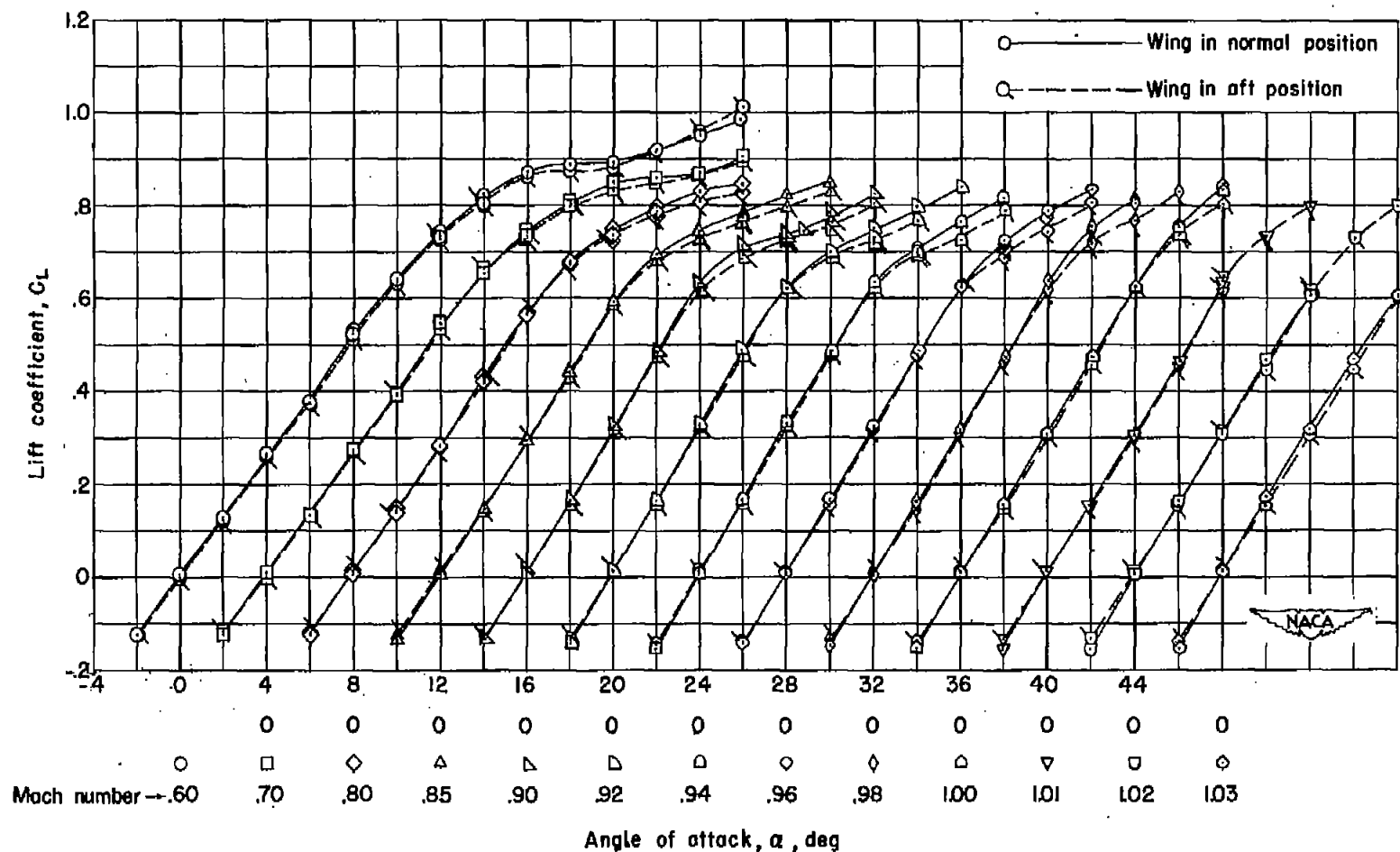


Figure 6.- Lift-curve comparison for wing-normal and wing-aft models.

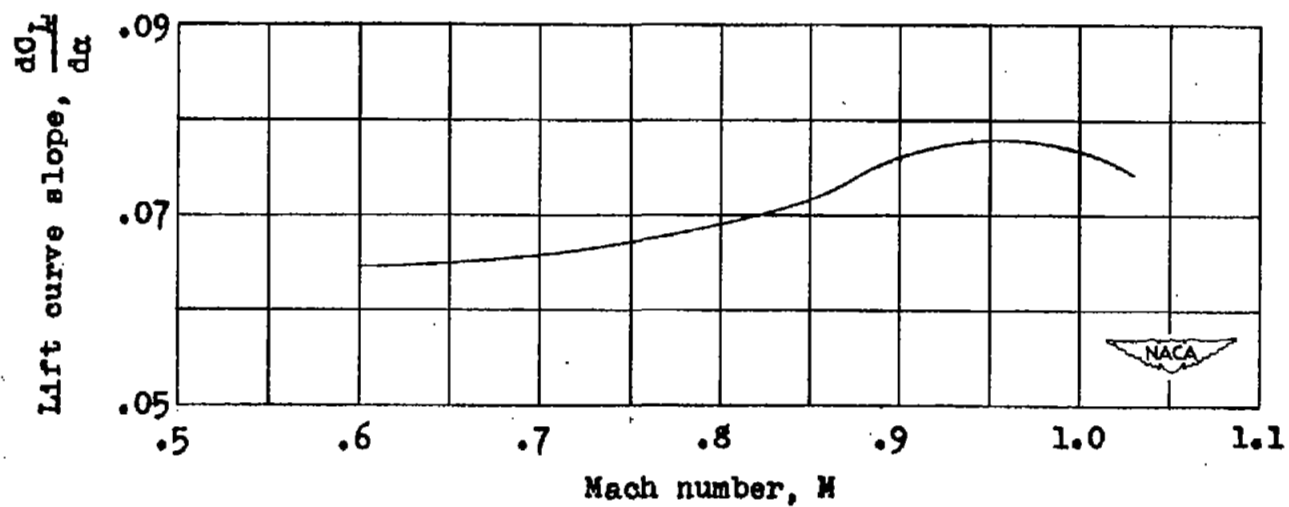


Figure 7.- Average lift-curve slope for wing-normal and wing-aft configurations from $C_L = 0$ to $C_L = 0.6$.

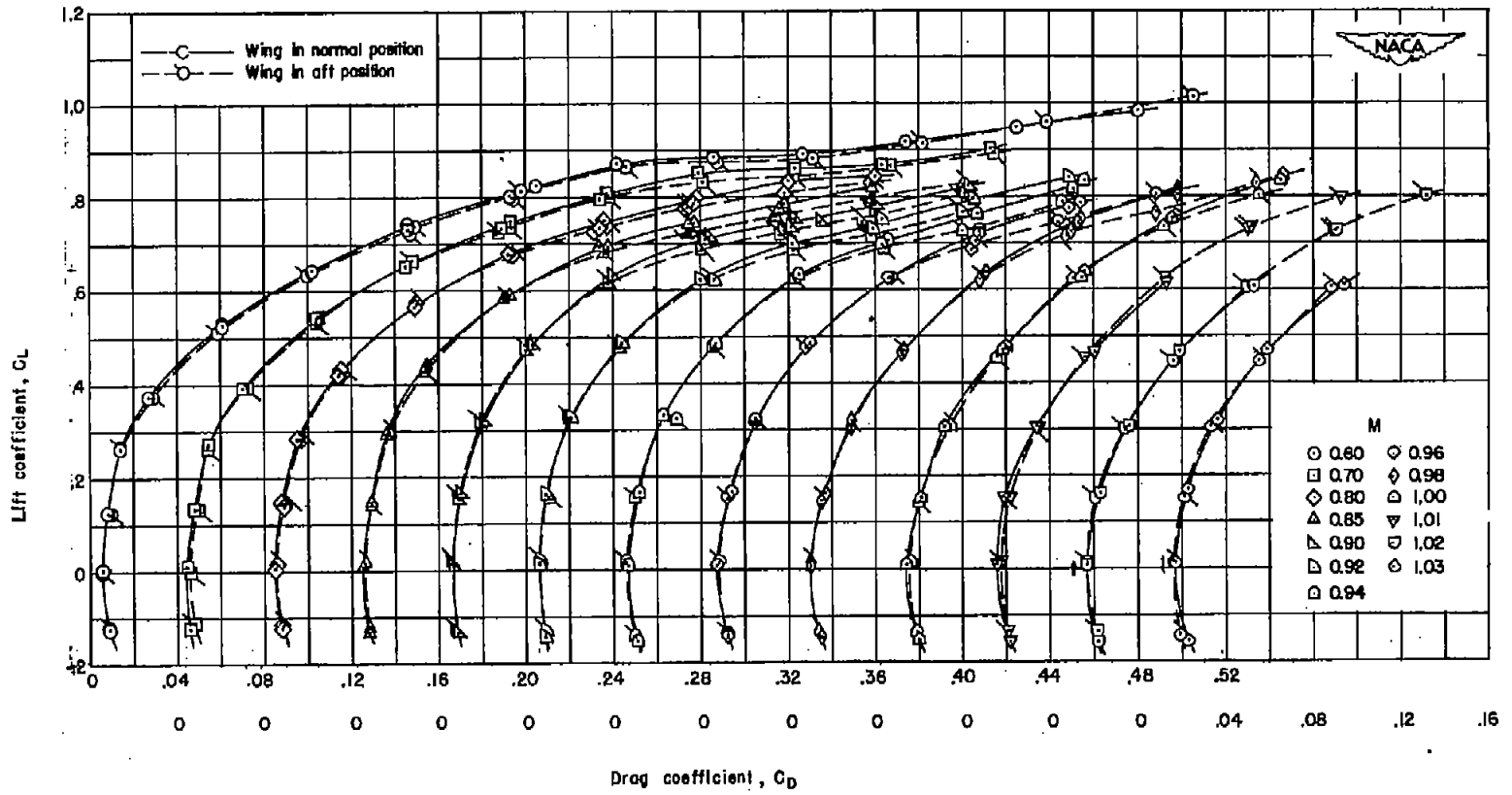


Figure 8.- Drag polar comparison for wing-normal and wing-aft models.

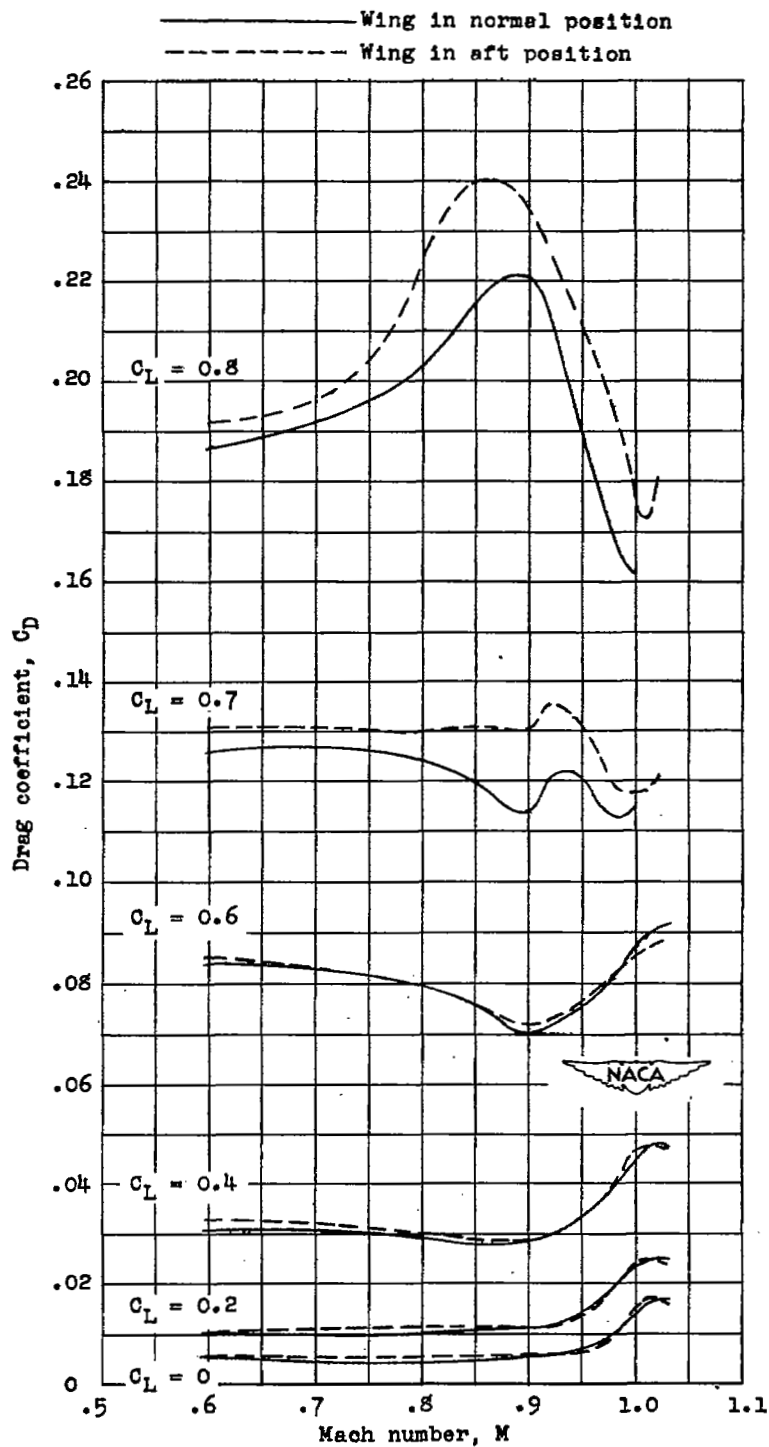


Figure 9.- Drag comparison for wing-normal and wing-aft models at several lift-coefficient values.

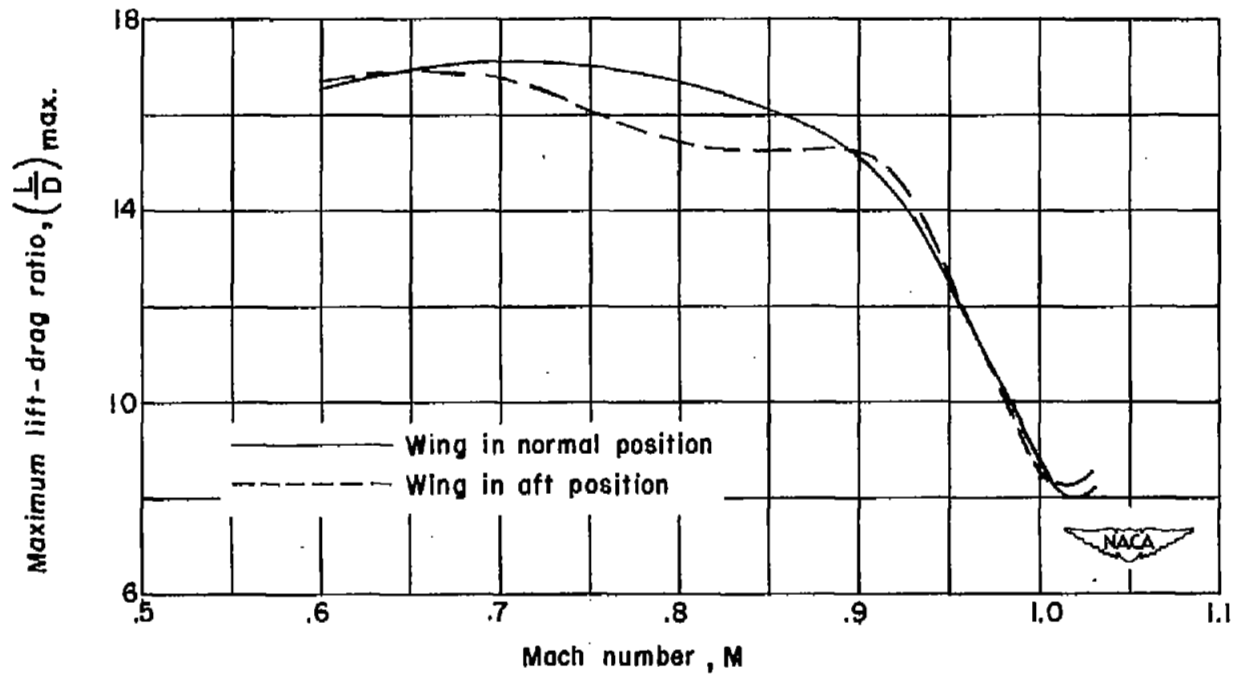


Figure 10.- Maximum lift-drag ratio comparison for wing-normal and wing-aft models. Drag data adjusted to the condition of free-stream pressure at the base.

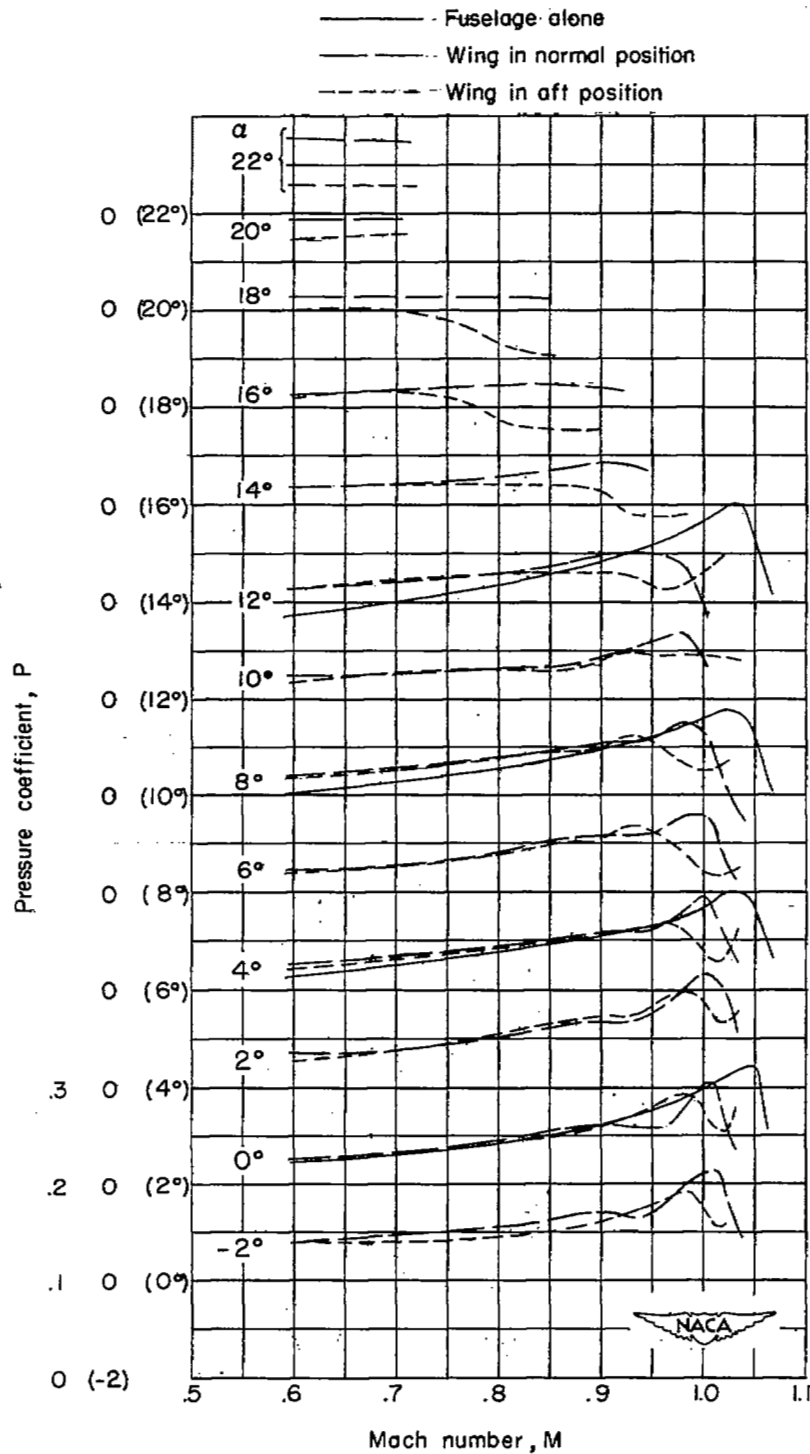


Figure 11.- Base-pressure coefficients obtained on the wing-normal and wing-aft configurations and on the body alone.

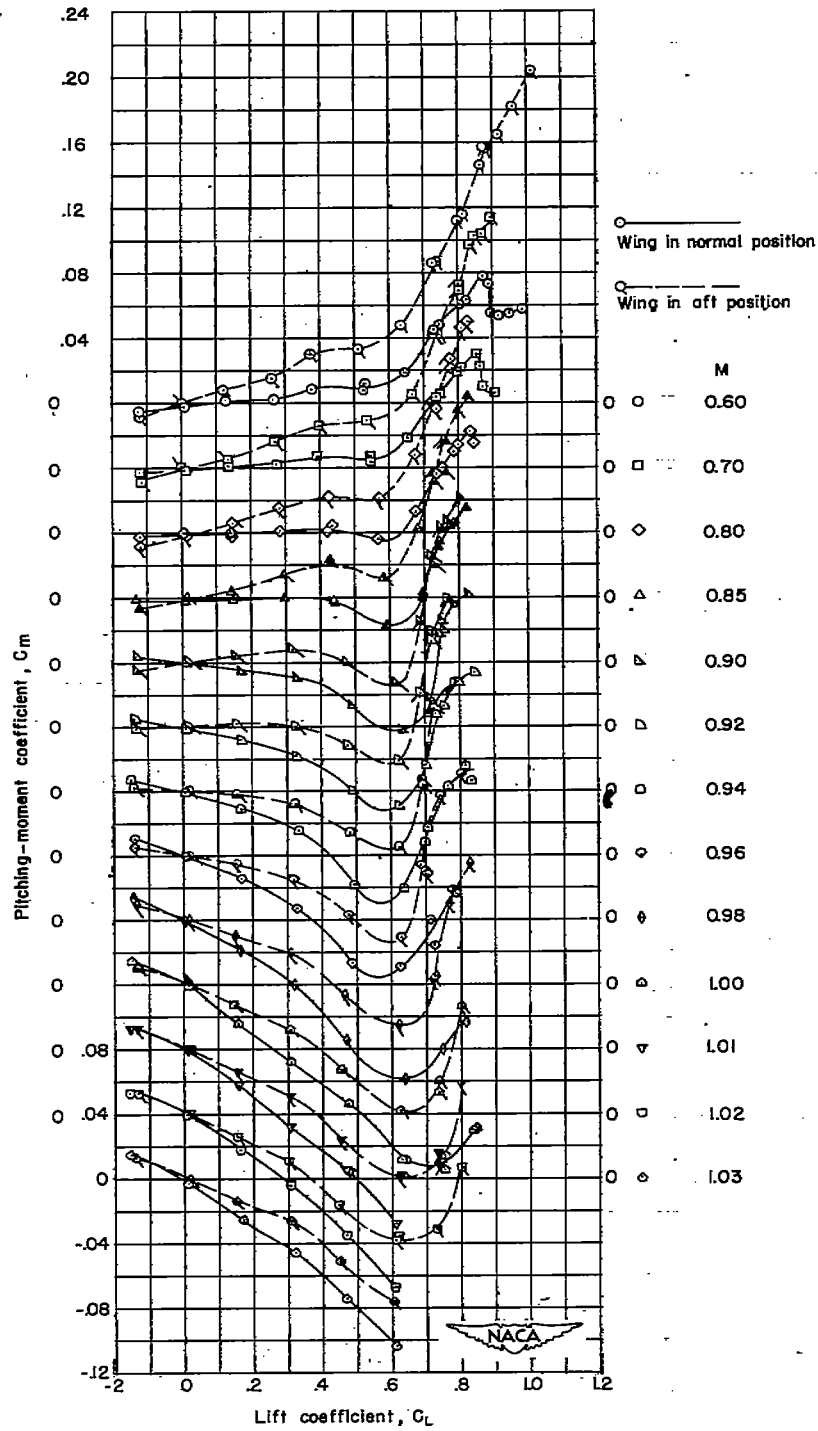


Figure 12.- Wing-fuselage pitching-moment comparison for wing-normal and wing-aft models.

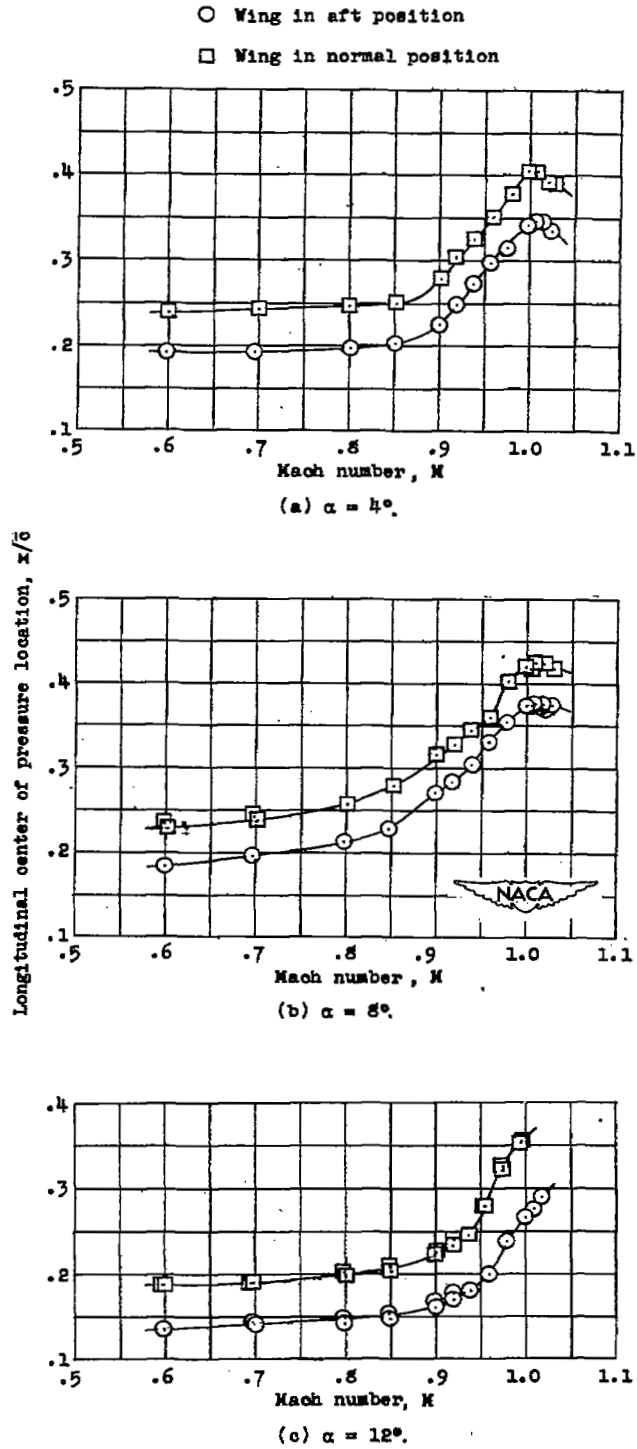


Figure 13.- Location of longitudinal center of pressure for wing-normal and wing-aft models at several angles of attack. (Complete configuration)

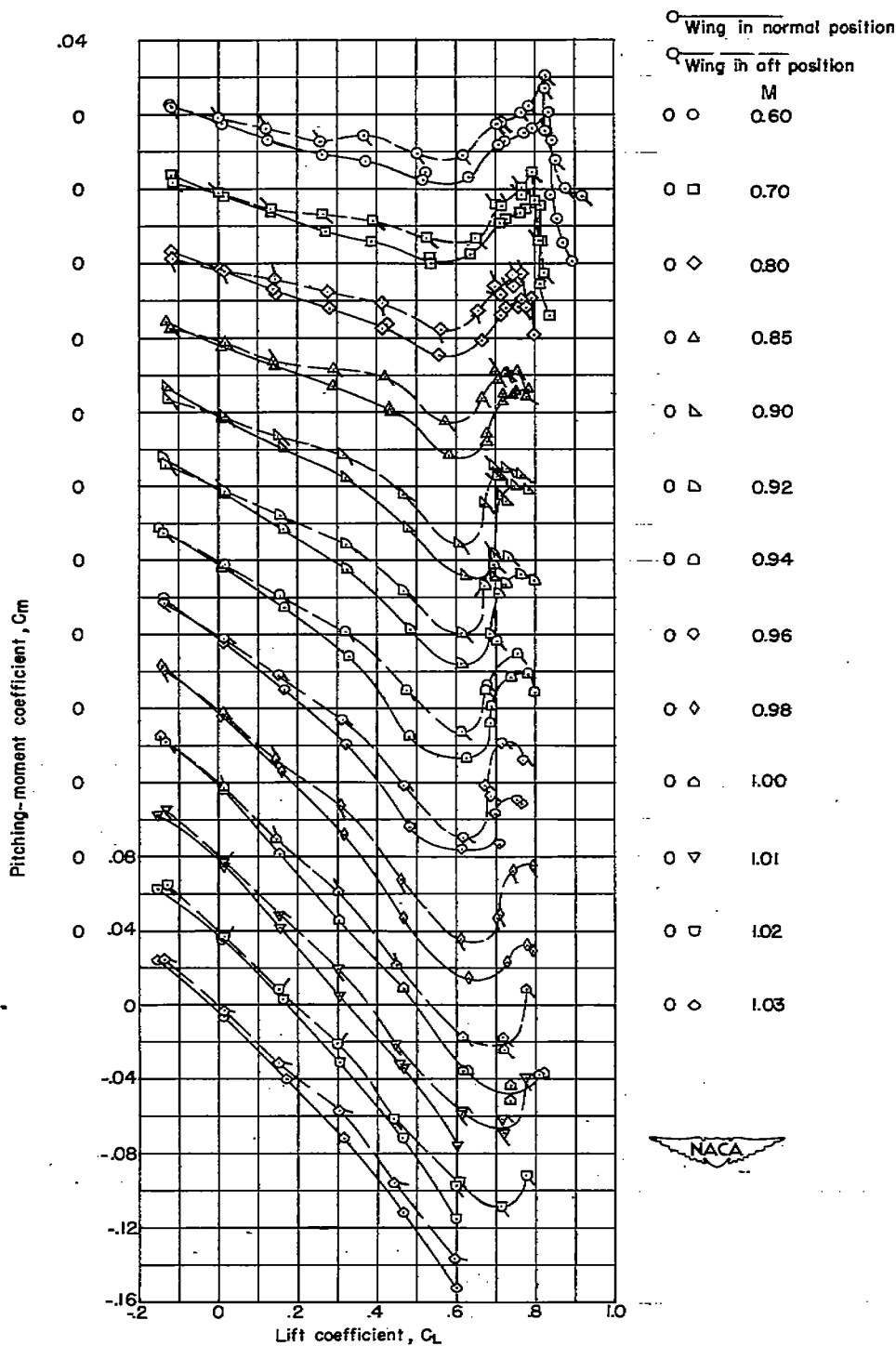


Figure 14.- Wing plus wing-fuselage interference pitching-moment comparison for wing-normal and wing-aft models.

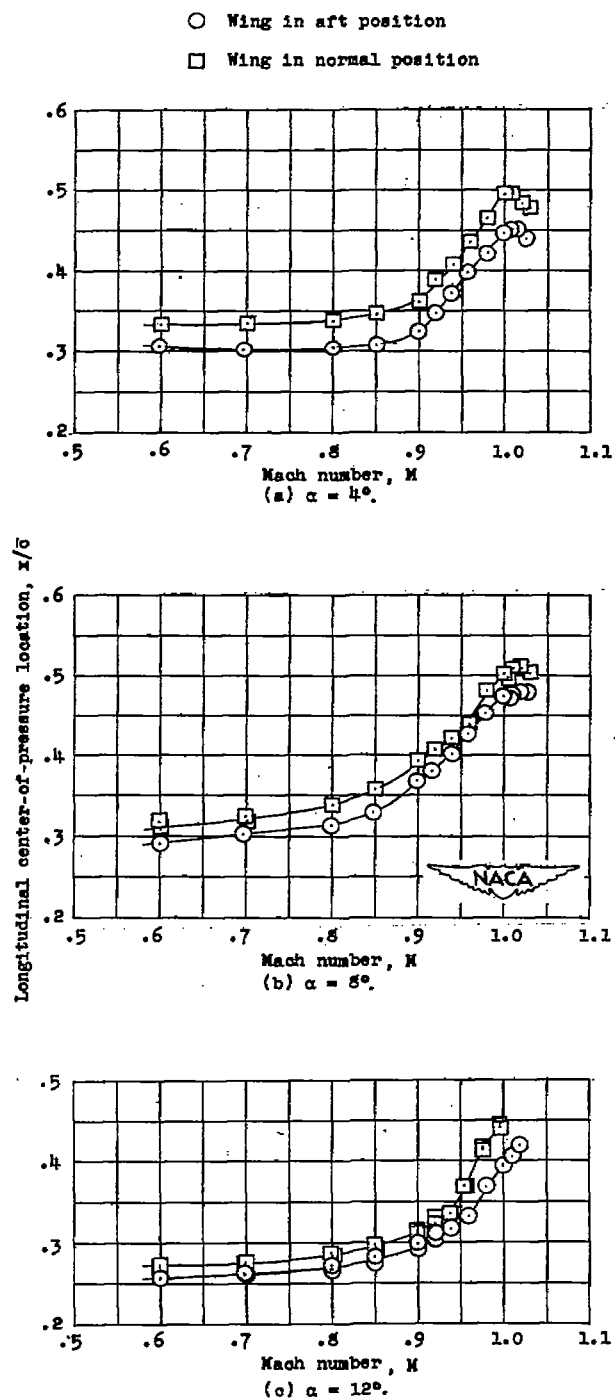


Figure 15.- Location of longitudinal center of pressure for wing-normal and wing-aft models at several angles of attack. (Wing plus wing-fuselage interferences)

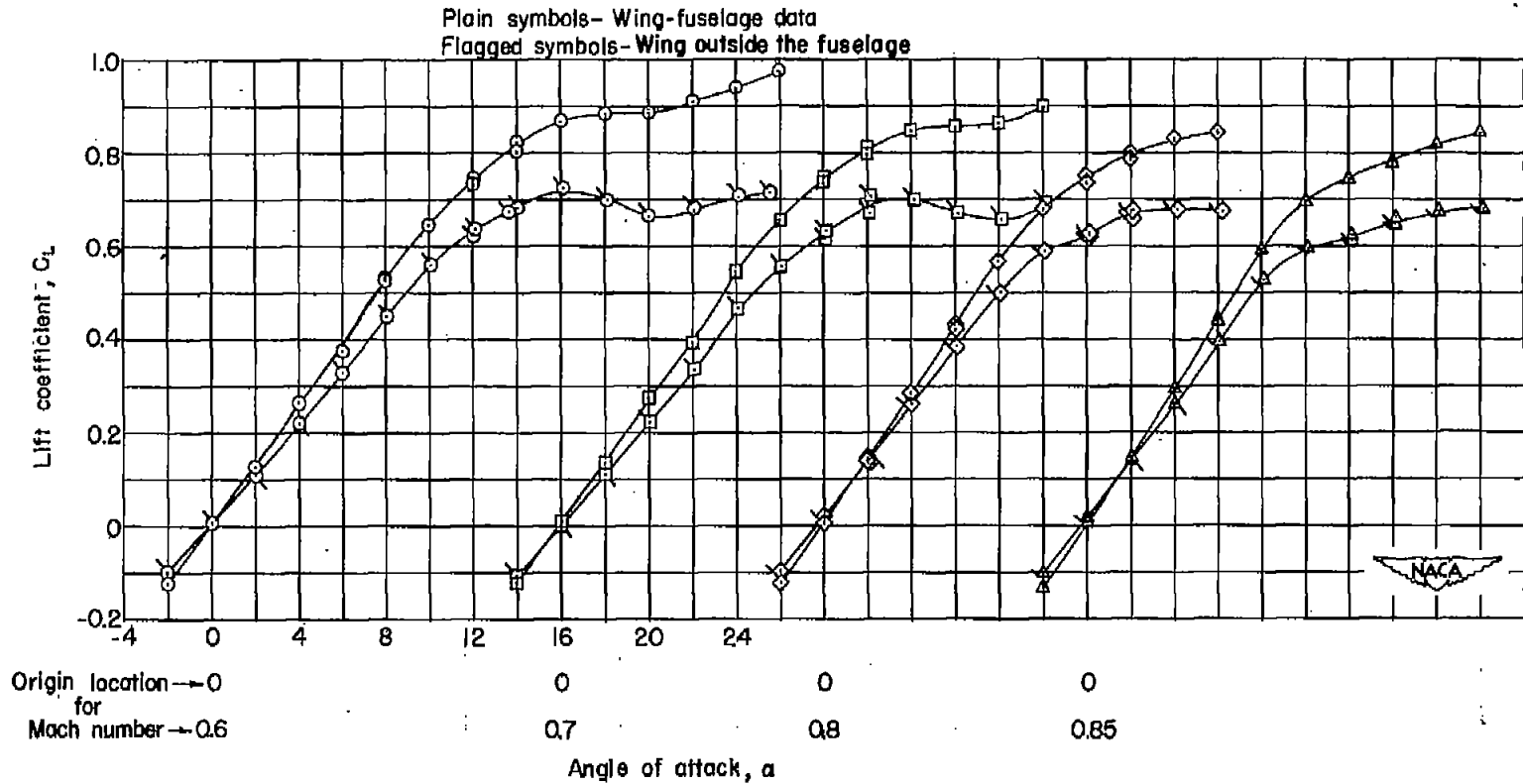
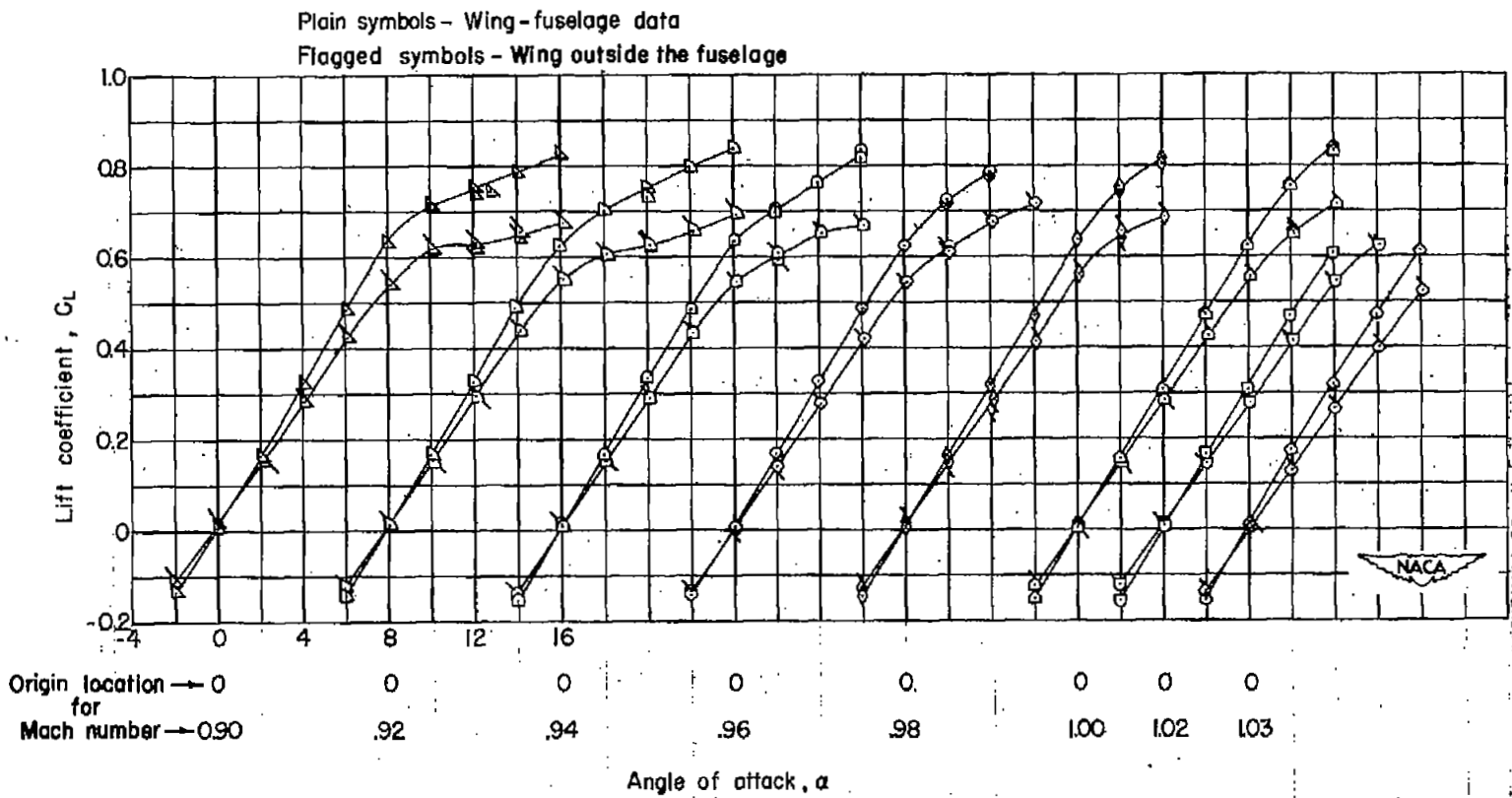
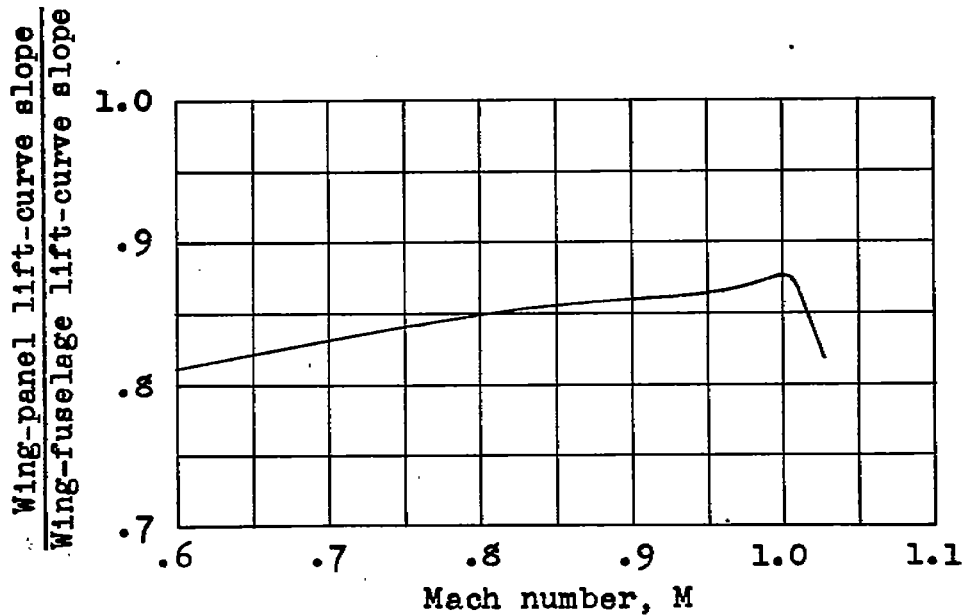


Figure 16.- Comparison of lift of the complete wing-fuselage configuration with lift of the wing outside of the fuselage.

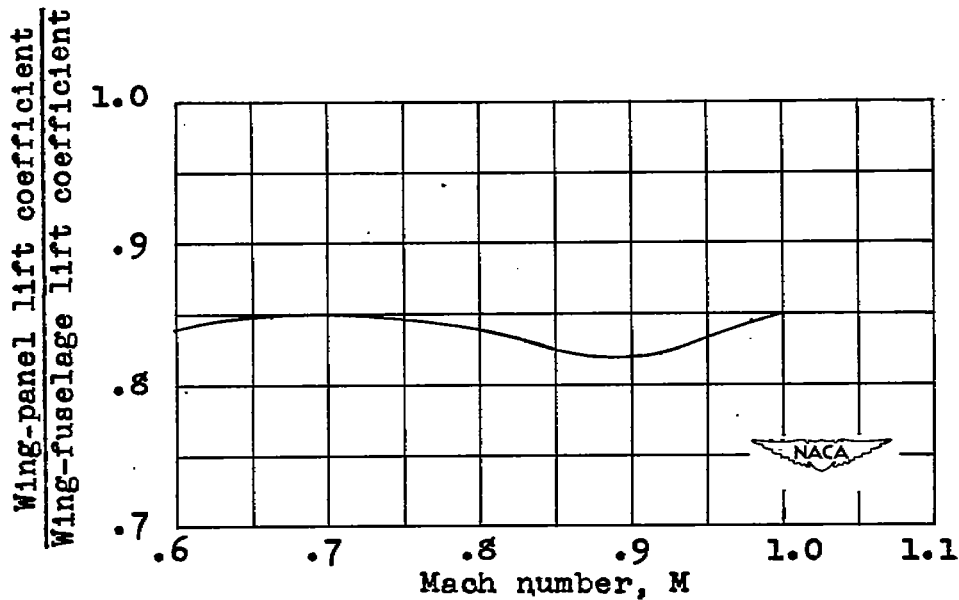


(b) Mach numbers 0.90 to 1.03.

Figure 16.- Concluded.

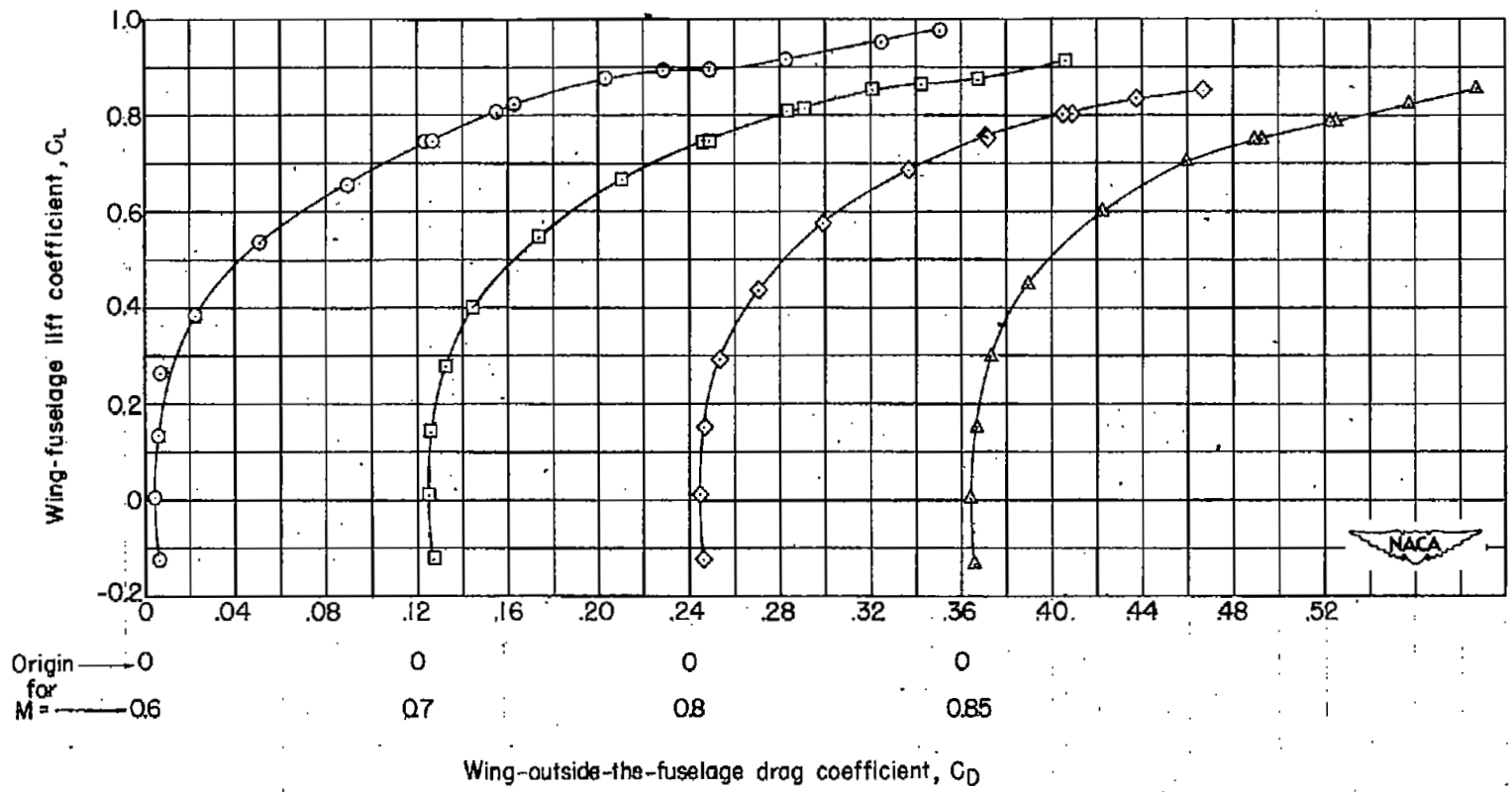


(a) Lift coefficient, 0.



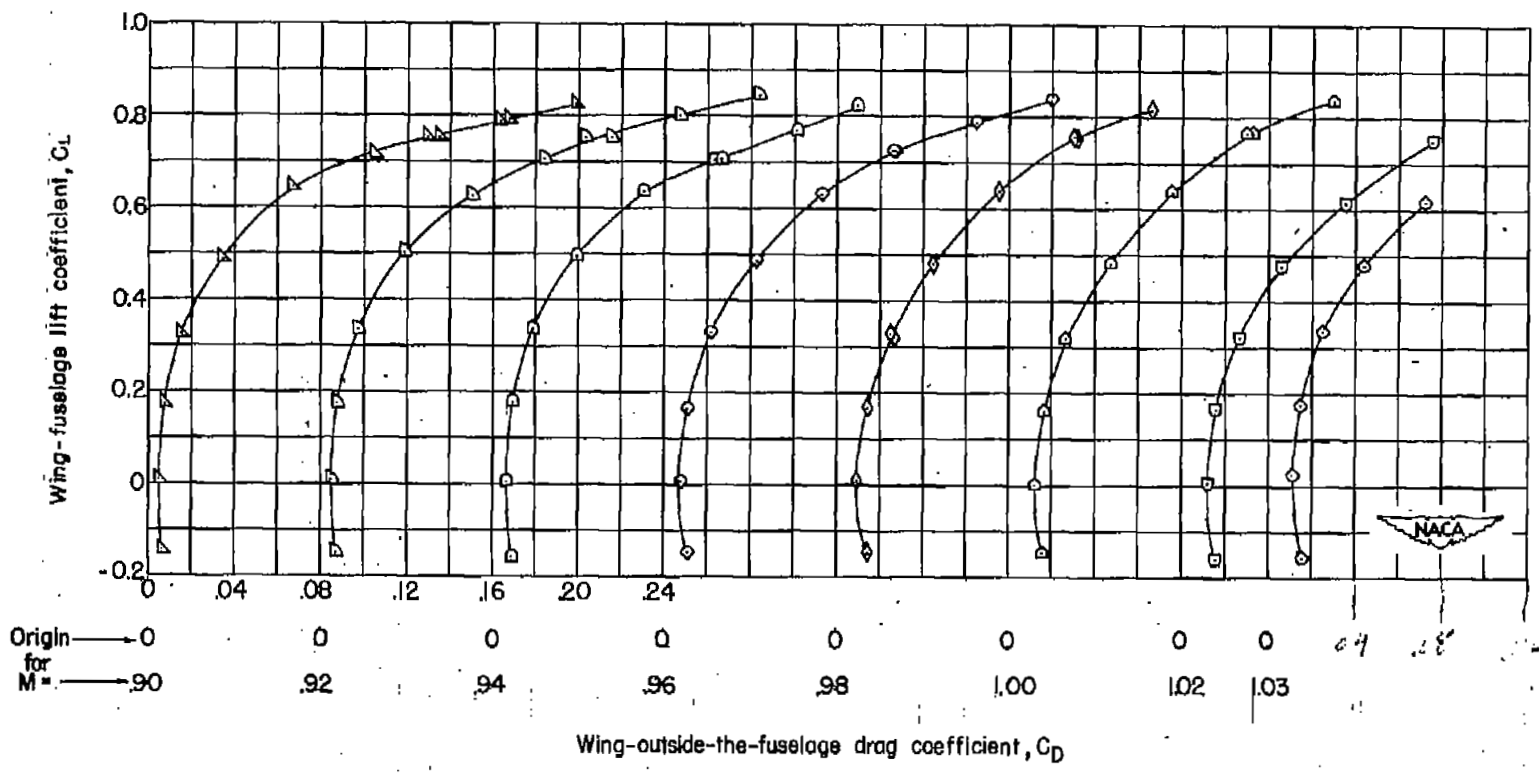
(b) Wing-fuselage lift coefficient, 0.8.

Figure 17.- Fraction of total lift load carried by the wing panel outside the fuselage.



(a) Mach numbers 0.60 to 0.85.

Figure 18.- Drag coefficient of the wing outside the fuselage as a function of wing-fuselage lift coefficient.



(b) Mach numbers 0.90 to 1.03.

Figure 18.- Concluded.

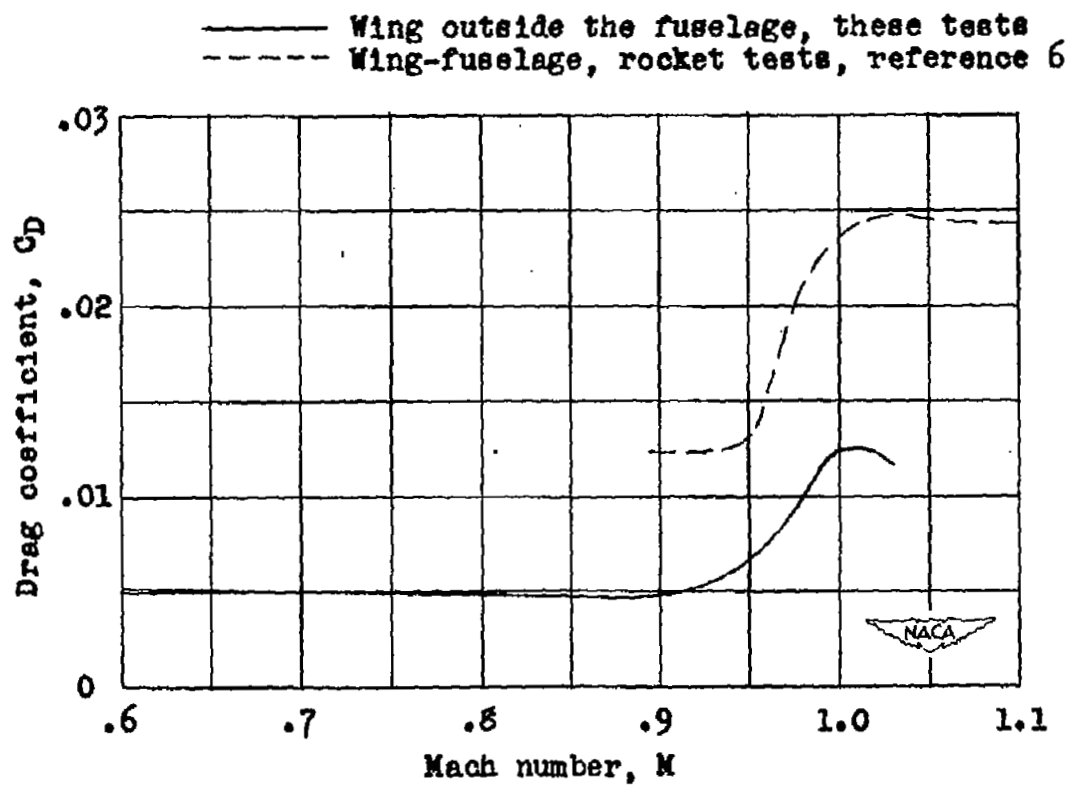


Figure 19.- Zero-lift drag coefficient.

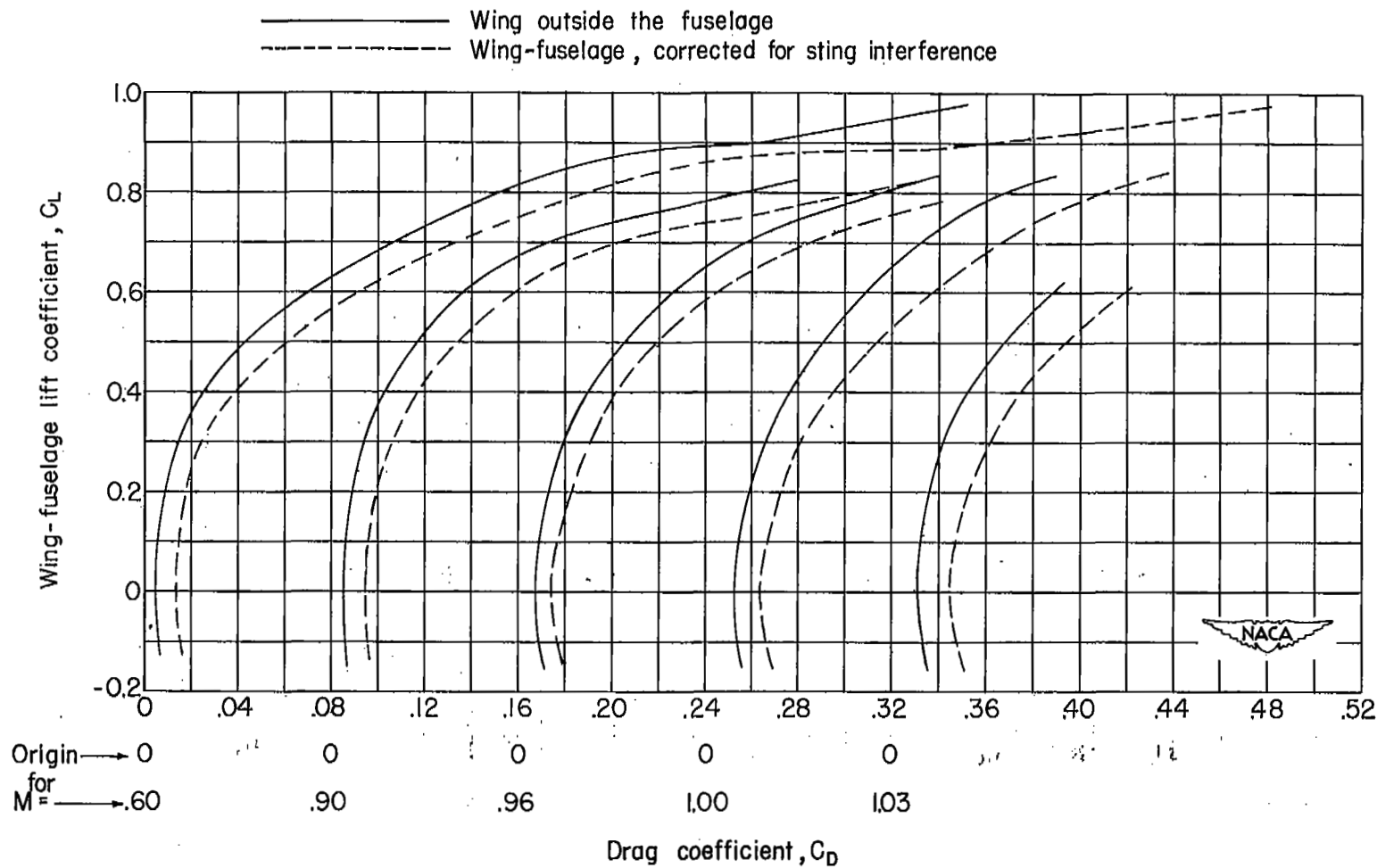
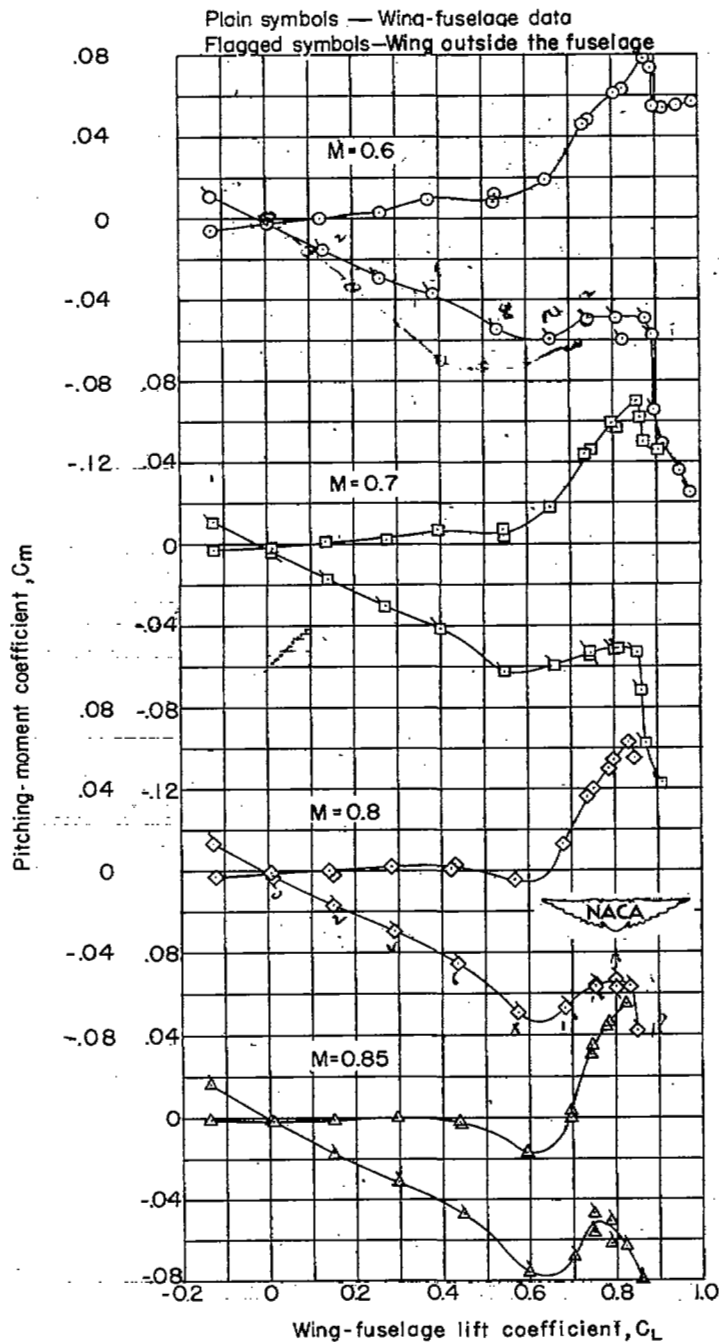


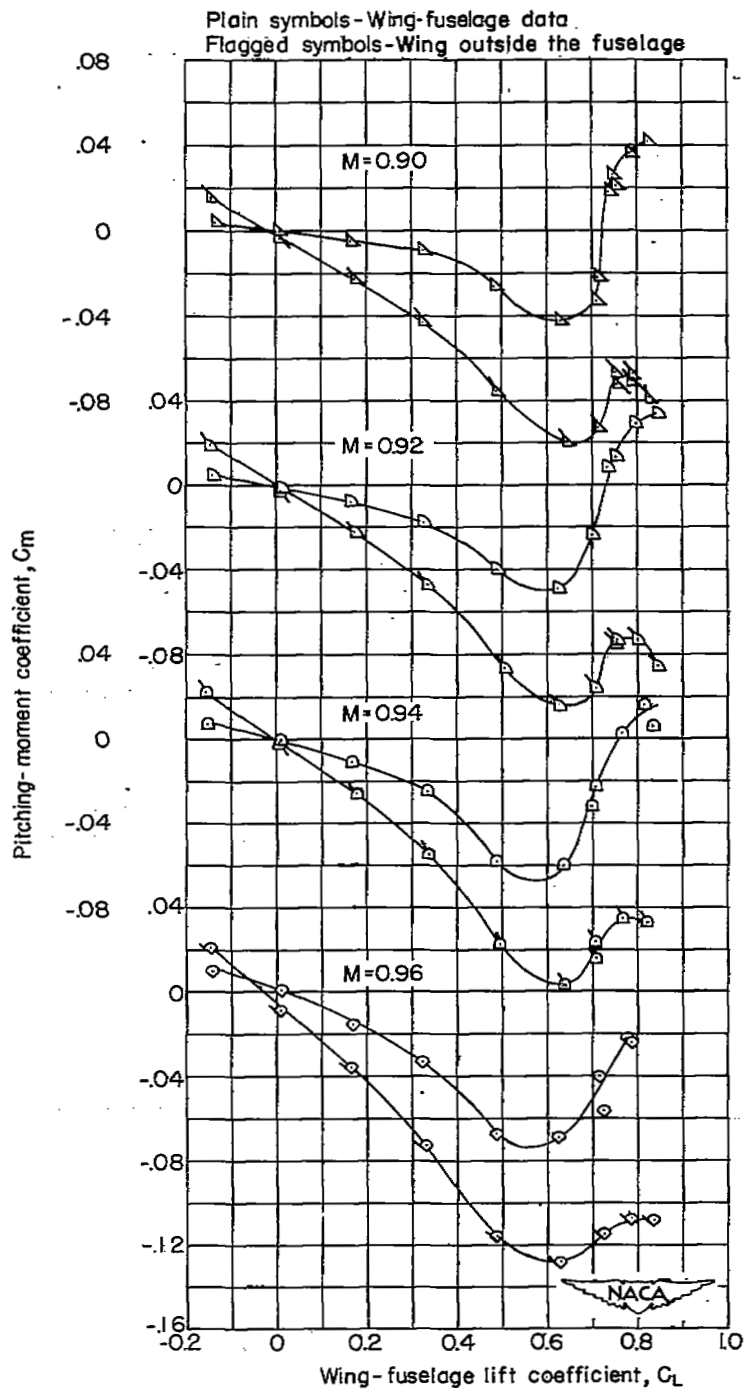
Figure 20.- Comparison at several Mach numbers of the drag coefficient of the wing outside the fuselage with the total drag coefficient (including estimated sting tare correction).



(a) Mach numbers 0.60 to 0.85.

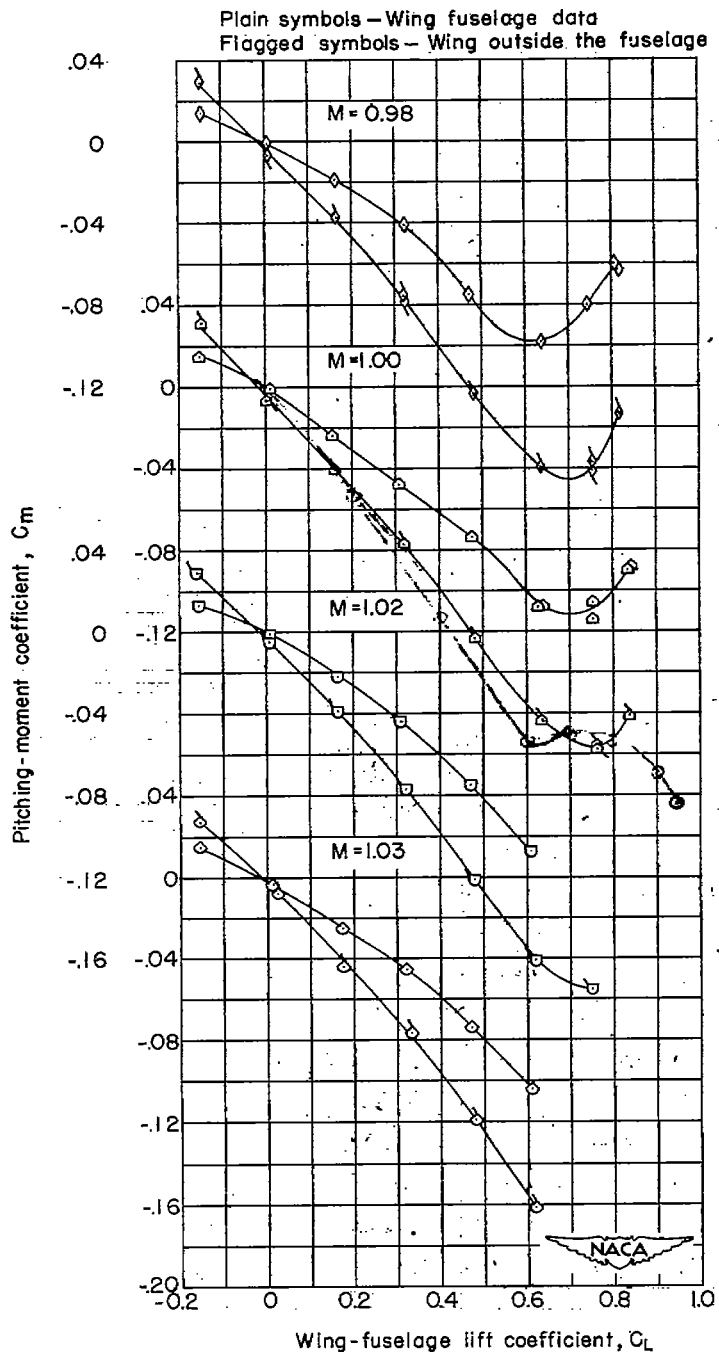
Figure 21.- Pitching moments of the complete wing-fuselage and of the wing outside of the fuselage as a function of wing-fuselage lift.

Wing - outside fuselage



(b) Mach numbers 0.90 to 0.96.

Figure 21.- Continued.



(c) Mach numbers 0.98 to 1.03.

Figure 21.- Concluded.

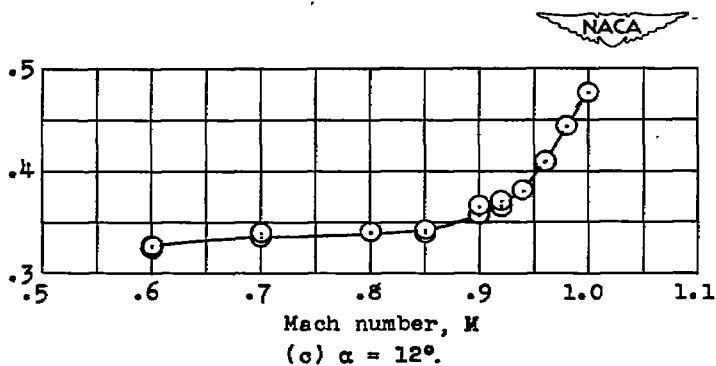
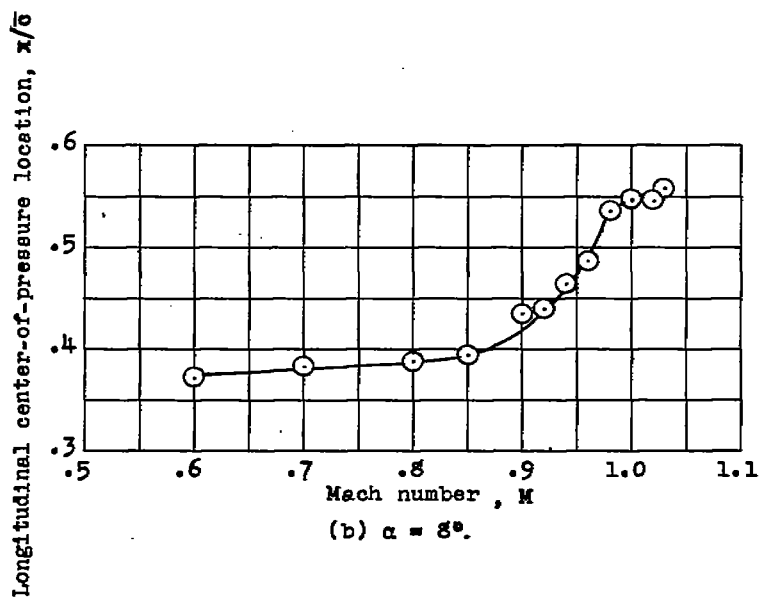
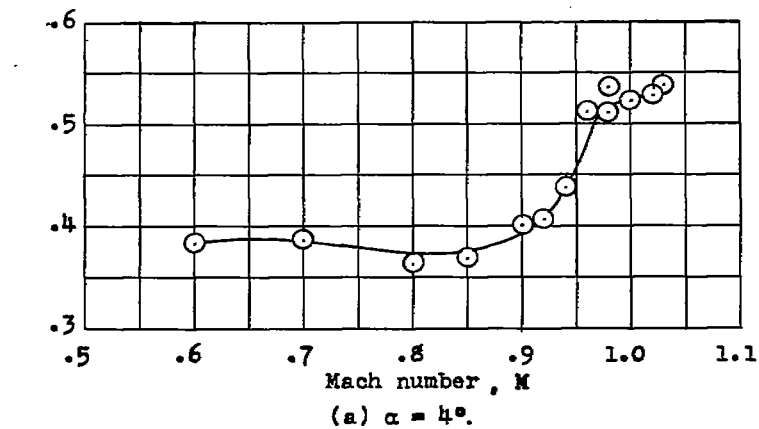


Figure 22.- Longitudinal center of pressure for the wing outside the fuselage at several angles of attack.

SECURITY INFORMATION

NASA Technical Library



3 1176 01436 9665

